iScience

CellPress
OPEN ACCESS

Article

Genomic and transcriptomic characterization of delta SARS-CoV-2 infection in free-ranging white-tailed deer (*Odocoileus virginianus*)

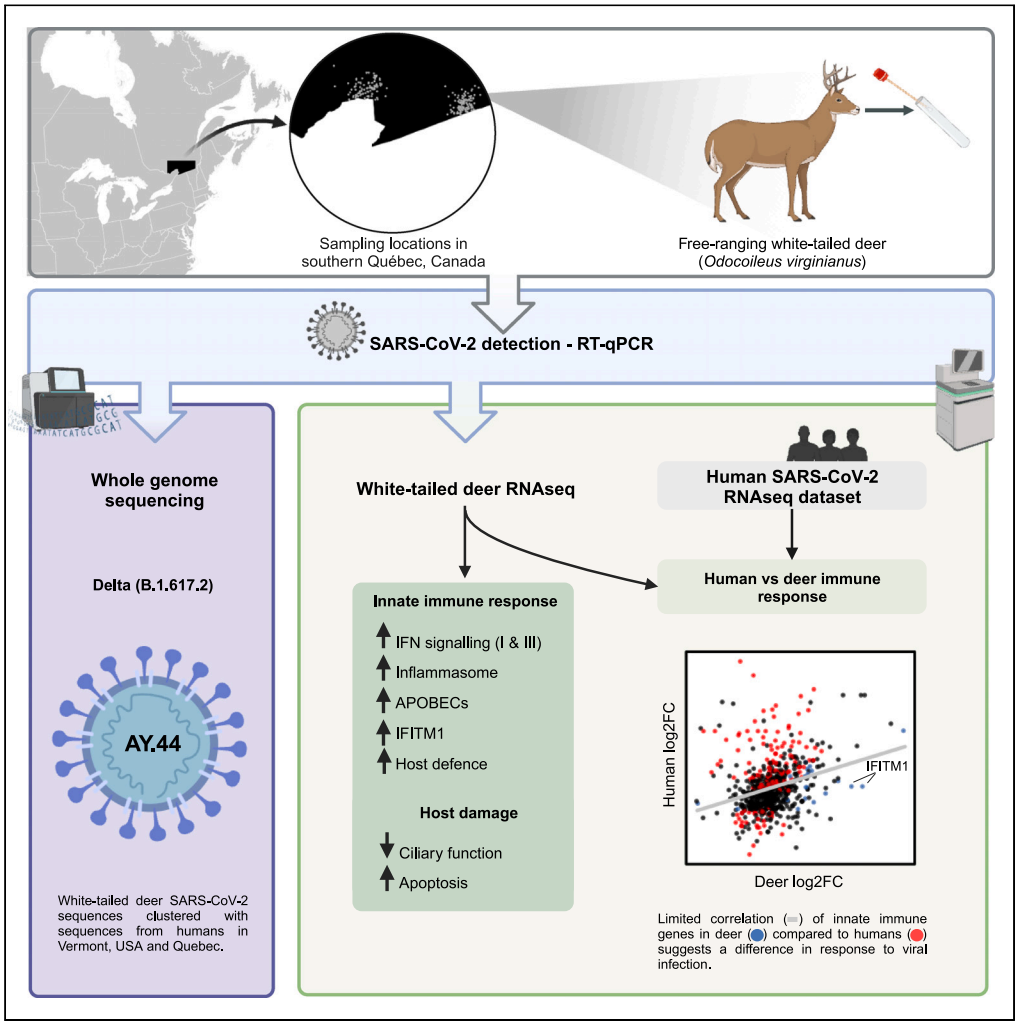

Jonathon D. Kotwa, Briallen Lobb, Ariane Massé, ..., Andrew C. Doxey, Bradley Pickering, Samira Mubareka

andrew.doxey@uwaterloo.ca (A.C.D.)
bradley.pickering@canada.ca (B.P.)
samira.mubareka@sunnybrook.ca (S.M.)

Highlights

Delta SARS-CoV-2 was detected in white-tailed deer from southern Quebec

Host expression patterns from naturally infected deer differed from humans

These deer show increased type I, III interferons, APOBECs and IFITM1 expression

Kotwa et al., iScience 26, 108319
November 17, 2023
https://doi.org/10.1016/j.isci.2023.108319

iScience

CellPress
OPEN ACCESS

Article

Genomic and transcriptomic characterization of delta SARS-CoV-2 infection in free-ranging white-tailed deer (*Odocoileus virginianus*)

Jonathon D. Kotwa,[1] Briallen Lobb,[2] Ariane Massé,[3] Marianne Gagnier,[3] Patryk Aftanas,[17] Arinjay Banerjee,[2,4,5,6,7] Andra Banete,[1] Juliette Blais-Savoie,[1] Jeff Bowman,[8] Tore Buchanan,[8] Hsien-Yao Chee,[1,9] Peter Kruczkiewicz,[10] Kuganya Nirmalarajah,[1] Catherine Soos,[11,12] Oksana Vernygora,[10] Lily Yip,[1] L. Robbin Lindsay,[13] Allison J. McGeer,[6,14] Finlay Maguire,[15,16,17] Oliver Lung,[10,18] Andrew C. Doxey,[2,*] Bradley Pickering,[10,19,20,*] and Samira Mubareka[1,6,21,*]

SUMMARY

White-tailed deer (WTD) are susceptible to SARS-CoV-2 and represent an important species for surveillance. Samples from WTD (n = 258) collected in November 2021 from Québec, Canada were analyzed for SARS-CoV-2 RNA. We employed viral genomics and host transcriptomics to further characterize infection and investigate host response. We detected Delta SARS-CoV-2 (B.1.617.2) in WTD from the Estrie region; sequences clustered with human sequences from October 2021 from Vermont, USA, which borders this region. Mutations in the S-gene and a deletion in ORF8 were detected. Host expression patterns in SARS-CoV-2 infected WTD were associated with the innate immune response, including signaling pathways related to anti-viral, pro- and anti-inflammatory signaling, and host damage. We found limited correlation between genes associated with innate immune response from human and WTD nasal samples, suggesting differences in responses to SARS-CoV-2 infection. Our findings provide preliminary insights into host response to SARS-CoV-2 infection in naturally infected WTD.

INTRODUCTION

White-tailed deer (*Odocoileus virginianus*) are considered a priority species for severe acute respiratory syndrome coronavirus 2 (SARS-CoV-2) surveillance in North America based on existing epidemiological and experimental evidence of SARS-CoV-2 exposure, infection, and transmission.[1–11] Multiple focally distributed human to white-tailed deer (WTD) spillover events have been observed, with initial whole genome sequencing (WGS) analyses revealing SARS-CoV-2 lineages in WTD that reflect those contemporaneously circulating in humans.[4,5,12] Multiple studies have also documented evidence for onward and sustained deer-to-deer transmission.[1,6,10,12,13] This includes the circulation of nearly extinct SARS-CoV-2 lineages (Alpha and Gamma) persisting in WTD in New York and Pennsylvania, USA, with a notable time lapse between the detection of these variants in humans and WTD.[1,6] In Ontario, Canada, we previously identified a highly divergent SARS-CoV-2 variant

[1]Sunnybrook Research Institute, Toronto, ON M4N 3M5, Canada
[2]Department of Biology, University of Waterloo, Waterloo, ON N2L 3G1, Canada
[3]Ministère de l'Environnement, de la Lutte contre les changements climatiques, de la Faune et des Parcs, Québec City, QC G1S 4X4, Canada
[4]Vaccine and Infectious Disease Organization, University of Saskatchewan, Saskatoon, SK S7N 5E3, Canada
[5]Department of Veterinary Microbiology, University of Saskatchewan, Saskatoon, SK S7N 5A2, Canada
[6]Department of Laboratory Medicine and Pathobiology, Temerty Faculty of Medicine, University of Toronto, Toronto, ON M5S 1A1, Canada
[7]Department of Biochemistry and Molecular Biology, Faculty of Medicine, University of British Columbia, Vancouver, BC V6T 1Z4, Canada
[8]Wildlife Research and Monitoring Section, Ontario Ministry of Natural Resources and Forestry, Peterborough, ON K9J 8M5, Canada
[9]Global Health Research Center and Division of Natural and Applied Sciences, Duke Kunshan University, Kunshan, Jiangsu 215316, China
[10]National Centre for Foreign Animal Disease, Canadian Food Inspection Agency, Winnipeg, MB R3E 3M4, Canada
[11]Ecotoxicology and Wildlife Health Division, Environment and Climate Change Canada, Saskatoon, SK S7N 3H5, Canada
[12]Department of Veterinary Pathology, Western College of Veterinary Medicine, University of Saskatchewan, Saskatoon, SK S7N 5E3, Canada
[13]National Microbiology Laboratory, Public Health Agency of Canada, Winnipeg, MB R3E 3L5, Canada
[14]Sinai Health System, Toronto, ON M5G 1X5, Canada
[15]Faculty of Computer Science, Dalhousie University, Halifax, NS B3H 4R2, Canada
[16]Department of Community Health & Epidemiology, Faculty of Medicine, Dalhousie University, Halifax, NS B3H 4R2, Canada
[17]Shared Hospital Laboratory, Toronto, ON M4N 3M5, Canada
[18]Department of Biological Sciences, University of Manitoba, Winnipeg, MB R3T 2N2, Canada
[19]Department of Veterinary Microbiology and Preventative Medicine, College of Veterinary Medicine, Iowa State University, Ames, IA 50011, USA
[20]Department of Medical Microbiology and Infectious Diseases, University of Manitoba, Winnipeg, MB R3T 2N2, Canada
[21]Lead contact
*Correspondence: andrew.doxey@uwaterloo.ca (A.C.D.), bradley.pickering@canada.ca (B.P.), samira.mubareka@sunnybrook.ca (S.M.)
https://doi.org/10.1016/j.isci.2023.108319

Table 1. Results from SARS-CoV-2 RT-PCR testing of nasal swabs and retropharyngeal lymph node tissue from white-tailed deer, in two sampling regions, southern Québec, Canada, November 6-8 2021

	Nasal Swabs		Retropharyngeal Lymph Nodes	
Sampling area	No. Tested	No. SARS-CoV-2 RNA Positive (%; 95% CI)	No. Tested[a]	No. SARS-CoV-2 RNA Positive (%; 95% CI)[a]
Dunham station, Estrie region, High deer density	150	4 (2.7; 0.8–6.9)	NA	NA
Browsburg station, Laurentides region, Low deer density	101	0 (0; 0–4.4)	104	0 (0; 0–4.3)
Total	251	4 (1.6; 0.5–2.2)	104	0 (0; 0–4.3)

See also Table S1.
[a]NA, not applicable.

circulating in WTD (B.1.641) with evidence of WTD-to-human transmission;[10] this finding supports concerns for the emergence and accumulation of mutations in SARS-CoV-2 while circulating in novel animal hosts.[14] This introduces the possibility of further divergent viral evolution and spillback into humans, potentially undermining the effectiveness of medical countermeasures such as antivirals and vaccines.[15–17]

The growing evidence of SARS-CoV-2 circulation among WTD in North America is suggestive of a new non-human maintenance population or reservoir for the virus. Despite this fundamental change to the ecology of SARS-CoV-2, there remains a dearth of knowledge about the course of infection in WTD, the host-immune response, and resultant evolutionary pressures. Experimental data suggest that WTD infected with SARS-CoV-2 exhibit few clinical signs, and pathology is limited.[3,7,9] This is in contrast to the spectrum of disease severity observed in humans, underscoring the potential for differing host responses between species. There is a need to integrate data on host-immune response with epidemiological and ecological insights to understand the extent to which WTD host response contributes to their potential role as a maintenance host,[18,19] and to discern the implications of species-adapted viruses for human health.

To try to address this we investigated SARS-CoV-2 infection among WTD in southern Québec, Canada as part of a broader pan-Canadian approach to investigate SARS-CoV-2 spillover into wildlife. We then employed viral genomics and host transcriptomics to further characterise SARS-CoV-2 in a novel and ecologically relevant host.

RESULTS

SARS-CoV-2 delta variant of concern detected in white-tailed deer in southern Québec

To discern the prevalence of SARS-CoV-2 in WTD in the region, 258 WTD were sampled in two areas from southern Québec, Canada between November 6–8 2021. The majority of the sampled WTD were adult (92%) and male (79%). We collected 251 nasal swabs and 104 retropharyngeal lymph nodes (RPLNs) and tested for the presence of SARS-CoV-2 ribonucleic acid (RNA) by reverse-transcription polymerase chain reaction (RT-PCR). Longitude and latitude data were obtained for 257 WTD. Chronic wasting disease was not detected in WTD in Quebec in 2021.[20]

Four nasal swabs were RT-PCR-positive, three of which were confirmed by the Canadian Food Inspection Agency (CFIA) and reported to the World Organization for Animal Health (WOAH) as the first cases of SARS-CoV-2 identified in Canadian wildlife on December 1, 2021 (Table S1).[21] Human RNase P was not detected in any of the positive nasal swabs, excluding contamination from human hosts. Of all nasal swabs, 1.6% (4/251; 95% CI 0.5–4.2%) were positive for SARS-CoV-2 RNA (Table 1); no RPLNs were positive; no RPLNs were available from deer with SARS-CoV-2 positive nasal swabs. All positive WTD were adults and three of the four were male. The four SARS-CoV-2-positive deer were harvested through licensed hunting activity in the high deer density region of Estrie (Figure 1).

Whole genome sequencing for SARS-CoV-2 conducted on three confirmed positive samples generated genome coverage of over 95% with equal to or greater than 10X coverage (mean depth from 1096.8 to 1894.8). On the fourth, higher cycle threshold (Ct) sample, 69.1% genome coverage with at least 10X coverage (mean depth of 116.5) was obtained (Table 2). Sequences were assigned to lineage AY.44, a sublineage of B.1.617.2 (Delta; 0.96–0.99 ambiguity score), while one sample could not be confidently assigned to a Pangolin lineage due to the large number of N bases (31%) in the consensus sequence. Phylogenetic analysis revealed that all sequenced samples clustered together and shared a most recent common ancestor with SARS-CoV-2 sequences from humans in Vermont, USA between 2021 and 10-14 and 2021-10-27 (Figure 2). Phylogenetic analysis of WTD derived SARS-CoV-2 sequences also revealed that all sequenced samples clustered together with WTD-derived SARS-CoV-2 sequences identified in the states of Iowa, Maine, Minnesota, New York, and Pennsylvania (Figure 3).

Mutations in the S gene and ORF8 detected in white-tailed deer-derived SARS-CoV-2 sequences

We observed multiple mutations in SARS-CoV-2 sequences derived from the four positive WTD samples (Table 3). None of the observed mutations were unique to WTD, however three mutations (open reading frame 1a [ORF1a]:L1853F, M:I82T, and ORF7a:T120I) are speculated to have evolved due to adaptation in WTD; only M:I82T was found in all four sequences.[1,22] Other mutations have been previously reported in WTD derived SARS-CoV-2 sequences from other regions (Table 3).

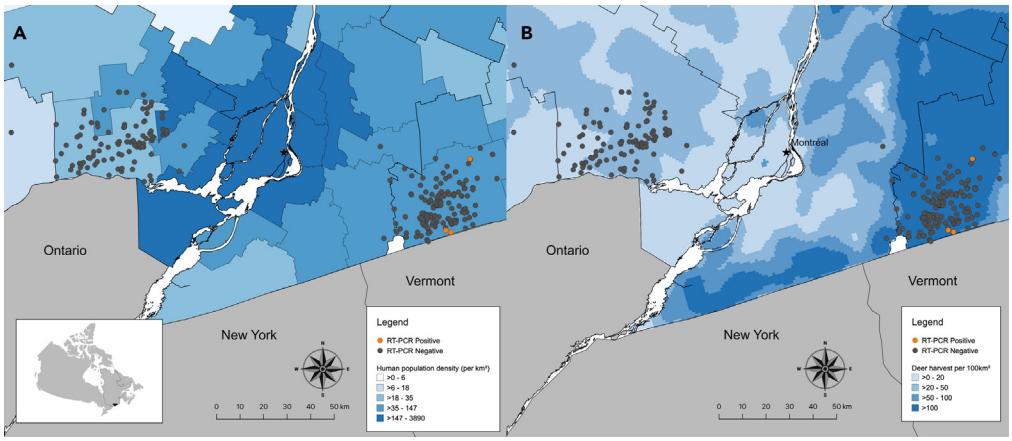

Figure 1. Locations of white-tailed deer (WTD) and SARS-CoV-2 RT-PCR test results in southern Québec, Canada

Map of southern Québec with locations of SARS-CoV-2 RT-PCR-positive (orange) and -negative (gray) WTD from November 6 - 8 2021 superimposed on (A) a choropleth map of human population density (per km^2) by regional county municipalities (thin gray boundaries) and (B) a heatmap of WTD harvest density per 100km^2 from 2020 as a proxy for deer population density. Inset shows the location of Québec (outlined) and study region (shaded black) within Canada. See also Figure S1.

Notably, two S gene mutations were observed in the WTD sequences: S:T22I in three samples and S:A27V in one sample. The S:T22I mutation was observed in only one closely related AY.44 sequence from a human from Quebec while S:A27V was not observed in closely related AY.44 sequences in GISAID. The S:T22I mutation has been observed in 16,628 GISAID sequences as of 2023-04-17 from a multitude of lineages. The S:A27V mutation has been observed in 5,889 GISAID sequences as of 2023-04-17. The S:G142D mutation, which is present in 64% of AY.44 sequences in GISAID (171,978/267,019 sequences as of 2023-04-17), is present in two samples as a minor variant (57% and 53% allele fraction, respectively). The S:G142D mutation is prevalent in many Delta sublineage sequences and present in 10,655,444 GISAID sequences as of 2023-04-17. Interestingly, the S:G1085R mutation, which is present in all four sequenced samples and related AY.44 sequences, is only present in 0.1% (279/267,019) in lineage AY.44 and has been identified in 2,574 GISAID sequences as of 2023-04-17.

An inframe deletion leading to a stop codon in the ORF8 was observed at S67/K68 (TCTA to T deletion at nucleotide position 28,092) in sample 4205. Additionally, an ORF8 inframe deletion of 6 amino acids at positions 61–66 and L60F mutation were observed in sample 4205 with an allele fraction of 59% (262/442 observations of TGTGCGTGGATGAGGCTGG to T at nucleotide position 28,072).

As most of the minor alleles were found in sample 4249, it is worth noting that this sample had 15 ambiguous genomic positions with otherwise high completeness (99.1%) and median coverage (1879X). This suggests that more than one SARS-CoV-2 genotype is present within the sequenced sample. This is attributable to either contamination or a mixed infection in the host. Demixing using Freyja v1.3 (https://github.com/andersen-lab/Freyja) revealed the sample was 99.4% AY.44 and 0.1% AY.98. However, no other samples in the same sequencing run contained the 4249-specific variants or were assigned to the AY.98 lineage making contamination less likely. Inter-run contamination is also unlikely since a new flow cell was used for each sequencing run and four different, alternating sets of 96 UD Indices were used to barcode the samples in the library pool to help mitigate index hopping. Moreover, all negative controls met quality control parameters, further suggesting contamination is unlikely. As AY.98 is closely related to AY.44 (differing by only 3 ORF1ab amino acid residues) and is inferred as low abundance, this suggests 4249 more likely represents a real mixed infection of two closely related AY.44 genomes.

Table 2. Read mapping statistics from nf-core/viralrecon analysis for four SARS-CoV-2 positive white-tailed deer nasal swab samples from southern Québec, Canada, November 6-8 2021

Nasal Swab ID	Genome Coverage (%)[a]	Mean Coverage Depth	Total Reads	Mapped Reads	0X positions	<10X positions	Virus name	GISAID Accession No.
4055	99.6	1227.1	375796	293802	121	121	hCoV-19/Canada/QC-WTD-qxic4055/2021	EPI_ISL_10168587
4204	69.1	116.5	503532	29803	3219	9245	QC failure, not uploaded	QC failure, not uploaded
4205	95.8	1096.8	370802	252101	674	1255	hCoV-19/Canada/QC-WTD-qxic4205/2021	EPI_ISL_10169675
4249	98.9	1894.8	583638	460000	69	314	hCoV-19/Canada/QC-WTD-qxic4249/2021	EPI_ISL_10170149

[a]Genome coverage was calculated as the proportion of Wuhan-Hu-1 (MN908947.3) reference positions with at least 10X read mapping depth.

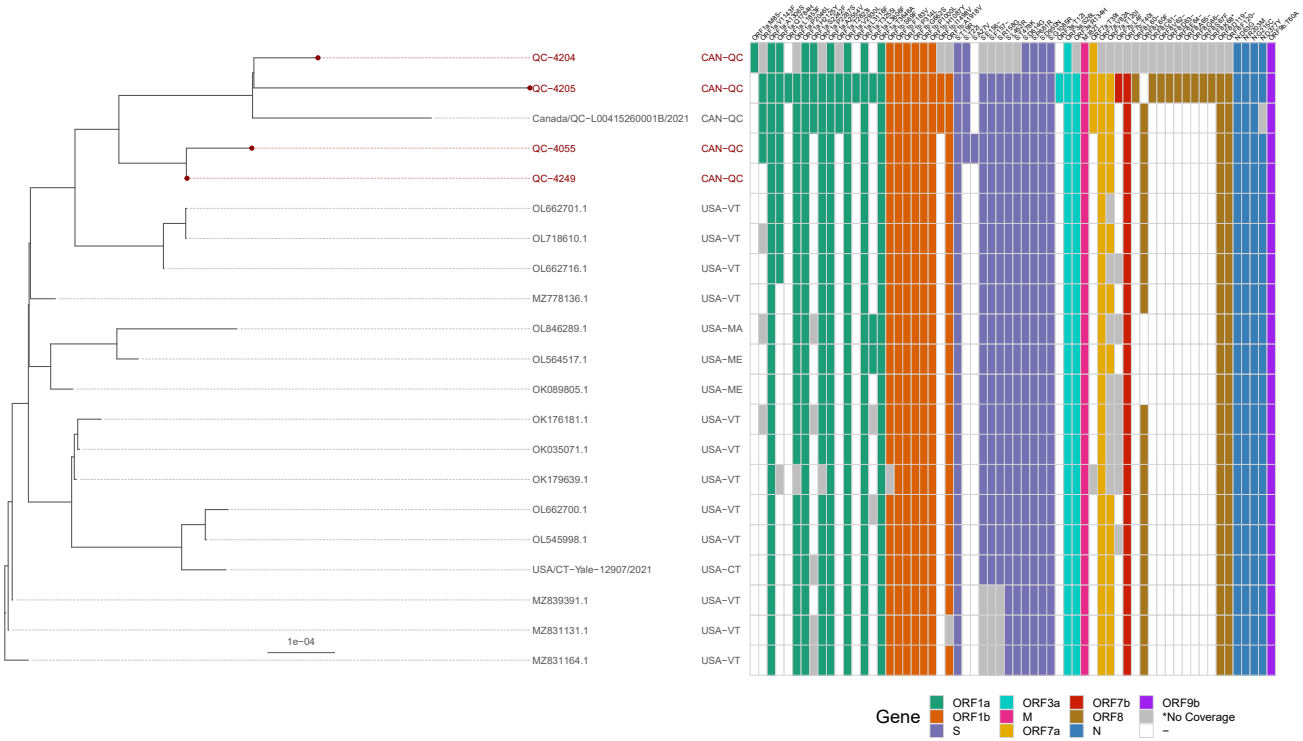

Figure 2. Whole-genome phylogenetic tree of four SARS-CoV-2 positive white-tailed deer (WTD) sequences and 17 closely related Canadian and American sequences identified by UShER analysis

IQ-TREE inferred the maximum-likelihood phylogenetic tree with a GTR+F+I + I + R5 substitution model (selected by IQ-TREE's ModelFinder) from a Nextalign multiple sequence alignment of the 4 WTD, 91 NCBI, 2 GISAID and Wuhan-Hu-1 (MN908947.3) sequences. The tree was manually pruned with BioPython to highlight distinct clades and amino acid mutation patterns. The tree was visualized using the ggtree R library. Amino acid (AA) substitutions and deletions in GISAID and WTD sequences were determined using Nextclade for visualization alongside the tree and other metadata. Some positions within sample 4204 had low or no coverage, however, despite the poor coverage of sample 4204, it still clustered with the other WTD.

Virus isolation

Two of the SARS-CoV-2-positive nasal swabs yielded viable virus when cultured in Vero E6 cells (Figure S2). Resultant sequences from the isolates were comparable to sequences from respective original nasal samples; key mutations found in the original nasal swab sample sequences were also identified in the sequences from the isolates. In addition, we noted several other mutations in the virus upon passaging in Vero E6 cells. Changes noted in 4055 after a single passage included S:R683W and a deletion in ORF 3a, V256-259. The S:R683W mutation has been previously attributed to adaptation in Vero E6 cell lines.[23,24] Five low coverage variants were lost in 4249, which may suggest selection for the more abundant genotype.

White-tailed deer nasal microbial community profile an indicator of SARS-CoV-2 infection

The WTD nasal swabs were sequenced by RNAseq, allowing for the taxonomic profiling of the nasal community with Kraken 2 and Bracken (Table S2). SARS-CoV-2 was detected in the reads from WTD samples that tested positive for SARS-CoV-2 (4055 and 4249) (Figure S3A), confirming the RT-PCR results. All swabs were collected and stored in media containing antibiotics and antifungals prior to analysis, which could impact bacterial and fungal profiles. However, the SARS-CoV-2 positive samples clustered together even when excluding SARS-CoV-2 transcriptomic data. SARS-CoV-2-negative WTD samples 4192 and 3719 had a divergent microbial profile compared to other negative samples, most notably for relative increases in *Cutibacterium acnes* compared to the other WTD nasal swabs (Figure S3A).

SARS-CoV-2 infection elicited antiviral, pro- and anti-inflammatory host response in white-tailed deer

We employed unbiased exploratory transcriptomic analysis to provide insights on WTD host response to SARS-CoV-2 infection. When considering the entire gene expression profile, the WTD samples that tested positive for SARS-CoV-2 (4055 and 4249) clustered apart from the negative samples (Figure S3B). The negative samples further clustered into two groups, with samples 4192 and 3719 clustering away from the rest (Figure S3B). This difference is likely not due to age, sex, or hunting zone since these factors are not unique to the two aforementioned negative samples.

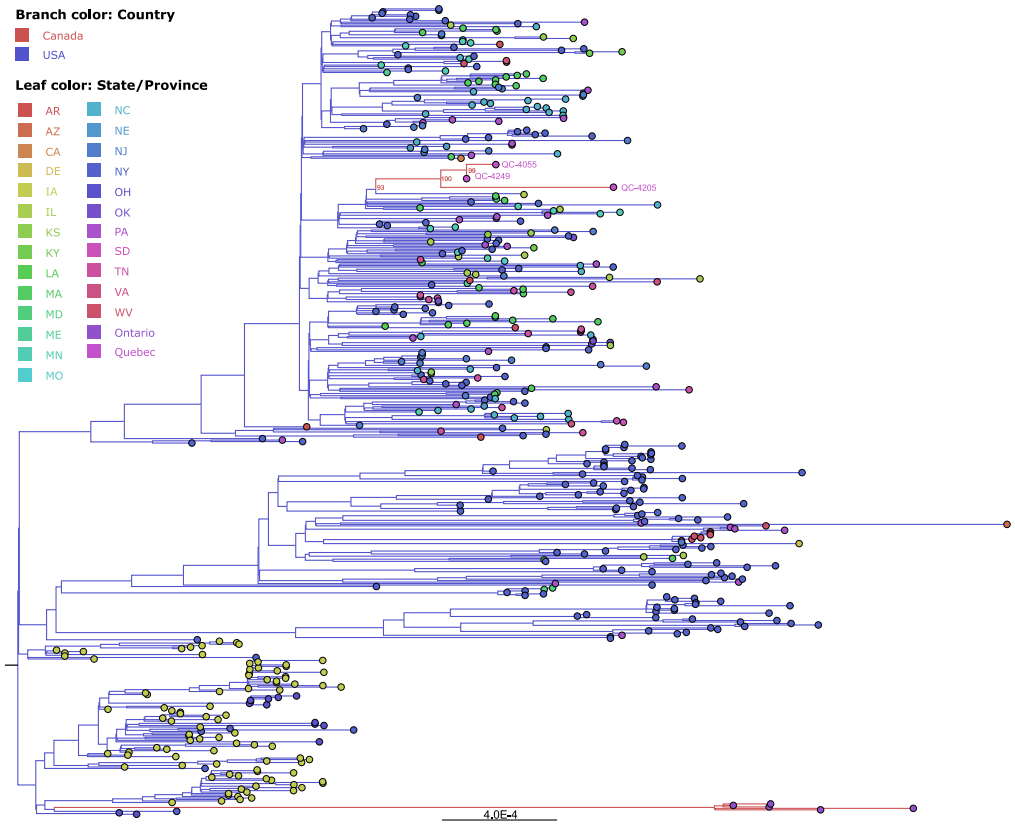

Figure 3. Maximum likelihood phylogenetic tree of the complete SARS-CoV-2 genomes isolated from white-tailed deer (WTD) and mule deer

Phylogeny was reconstructed using IQ-TREE under the GTR+F+I + R4 substitution model. The three high-coverage samples from Québec WTD are labeled on the tree. Branches of the phylogenetic tree are colored by the country of origin and the leaf markers are colored by the state or province of the sequence record origin. The tree is rooted to the outgroup sequence, Wuhan-Hu-1, MN908947.3 (not shown). Ultrafast bootstrap support values are shown at the node of the Québec WTD clade.

Differential expression analysis identified 316 significant differentially expressed genes (DEGs) (adjusted $p < 0.05$, >1-fold change), spanning 194 upregulated DEGs and 122 downregulated DEGs (Figures 4A and 4B and Table S3). Top expressed genes included *LOC110149600* (an inferred ortholog of human *interferon induced transmembrane protein 1* [*IFITM1*]), *LOC110149612* (inferred *IFITM1*), *2′-5′-oligoadenylate 2* (*OAS2*), *hematopoietic SH2 domain containing* (*HSH2D*), and *apolipoprotein B MRNA editing enzyme catalytic subunit 3H* (*APOBEC3H*) (Table 4 and Figure 4B). Notably, several significant DEGs appear to have duplications of human immune genes, including *IFITM1*, *interferon, alpha-inducible protein 27 like 2A* (*IFI27L2A*), *C4a*, *heterogeneous nuclear ribonucleoprotein A1* (*HNRNPA1*), and *XIAP associated factor 1* (*XAF1*). Upon narrowing down to known SARS-CoV-2 viral attachment and entry factors that have been identified as important for human COVID-19 infection (e.g., *angiotensin converting enzyme 2* [*ACE2*] and *transmembrane serine protease 2* [*TMPRSS2*]), only *sialic acid binding Ig like lectin 1* (*SIGLEC1*) was significantly upregulated in the WTD samples (Figure S4).

DEG function enrichment analysis using the Database for Annotation, Visualization and Integrated Discovery (DAVID) (Tables S3, S4, S5, and S6) revealed a change in the expression of key host factors in cellular innate immune response (interferon [IFN] signaling, inflammasome, APOBECs), damage (ciliary function and apoptosis), and permissivity (receptors, attachment, and entry factors) in RT-PCR-positive vs. RT-PCR-negative WTD. Significantly enriched Gene Ontology terms among up-regulated DEGs included defense response to virus, apoptotic process, innate immune response, inflammatory response, and chemotaxis, while down-regulated DEGs were involved in microtubule-mediated movement, axonemal dynein complex assembly, and ATP binding (Figure 4C). In humans and mice, orthologs of upregulated WTD DEGs are known to play important roles in type I and type III IFN signaling (e.g., *interferon regulatory transcription factor 3* [*IRF3*], *IRF4*, *IRF5*, *IRF7*, *IRF9*, *interferon lambda 3* [*IFNλ3*], *signal transducer and activator of transcription 2* [*STAT2*], *IFITM1*, *IFITM2*, *IFITM3*, *interferon alpha inducible protein 6* [*IFI6*], *IFI27L2A*), complement activation (e.g., *C2*, *C4a*), nucleic acid detection (e.g., *DExH-box helicase 58* [*DHX58*]), immune cell recruitment (e.g., *colony stimulating factor 1* [*CSF1*], *CC motif chemokine Receptor 1* [*CCR1*], *CXC motif chemokine receptor 2* [*CXCR2*], *RHO family interacting cell polarization regulator 2* [*RIPOR2*]), apoptosis (e.g., *engulfment and cell motility* [*ELMO*], *BH3 interacting domain death agonist* [*BID*], *XAF1*, *deoxyribonuclease 1 Like 3* [*DNASE1L3*]), and host defense (e.g., *bone marrow stromal cell antigen 2* [*BST2*], *Z-DNA binding protein 1* [*ZBP1*], *OAS2*, *adenosine deaminase RNA specific* [*ADAR*]). Orthologous DEGs that were

Table 3. Summary of mutations leading to amino acid changes found in sequences from four SARS-CoV-2 positive white-tailed deer nasal swab samples from southern Québec, Canada, November 6-8 2021

Gene	Amino Acid Mutation	Nucleotide Mutation	Nasal Swab ID(s)	Max Allele Fraction (%)[a]	Major Variant?[b]	Found in other white-tailed deer SARS-CoV-2 sequences[c]
orf1ab	ΔM85	TATG517T	4204	88.9	Yes	No
orf1ab	V1143F	G3692T	4055; 4205; 4249	100	Yes	No
orf1ab	A1306S	G4181T	4055; 4204; 4205; 4249	100	Yes	Yes
orf1ab	Q1784H	G5617T	4055; 4204; 4205; 4249	100	Yes	No
orf1ab	L1853F	C5822T	4205	91.4	Yes	Yes
orf1ab	P2046L	C6402T	4055; 4205; 4249	100	Yes	Yes
orf1ab	H2125Y	C6638T	4055; 4204; 4205; 4249	100	Yes	Yes
orf1ab	S2224F	C6936T	4249	26.1	No	Yes
orf1ab	S2242F	C6990T	4204; 4205	100	Yes	Yes
orf1ab	P2287S	C7124T	4055; 4205; 4249	100	Yes	Yes
orf1ab	A2554V	C7926T	4055; 4204; 4205; 4249	100	Yes	Yes
orf1ab	T2823I	C8733T	4205	100	Yes	No
orf1ab	V2930L	G9053T	4055; 4204; 4205; 4249	100	Yes	Yes
orf1ab	L3116F	C9611T	4205	99.1	Yes	Yes
orf1ab	T3255I	C10029T	4055; 4204; 4205; 4249	100	Yes	Yes
orf1ab	L3606F	G11083T	4204; 4205; 4249	100	Yes	Yes
orf1ab	T3646A	A11201G	4055; 4204; 4205; 4249	100	Yes	Yes
orf1ab	T4467I	C13665T	4205	98.5	Yes	Yes
orf1ab	I4562M	A13951G	4249	35.9	No	No
orf1ab	N4583K	T14014G	4055; 4204; 4205; 4249	100	Yes	Yes
orf1ab	H5401Y	C16466T	4055; 4204; 4205; 4249	100	Yes	Yes
orf1ab	I6162T	T18750C	4055; 4249	99.7	Yes	No
orf1ab	T6249I	C19011T	4205	99.7	Yes	Yes
orf1ab	V6265A	T19059C	4249	37.5	No	No
orf1ab	T6436I	C19572T	4205	100	Yes	Yes
orf1ab	T6775I	C20589T	4055; 4205	100	Yes	Yes
S	T19R	C21618G	4055; 4204; 4205; 4249	100	Yes	Yes
S	T22I	C21627T	4055; 4204; 4205; 4249	100	Yes	Yes
S	A27V	C21642T	4055; 4249	100	Yes	Yes
S	G142D	G21987A	4055; 4249	57.6	No	Yes
S	E156G, ΔFR157-158	GAGTTCA22028G	4055; 4205; 4249	100	Yes	Yes
S	L452R	T22917G	4055; 4205; 4249	100	Yes	Yes
S	T478K	C22995A	4055; 4249	100	Yes	Yes
S	D614G	A23403G	4055; 4204; 4205; 4249	100	Yes	Yes
S	P681R	C23604G	4055; 4204; 4205; 4249	100	Yes	Yes
S	D950N	G24410A	4055; 4204; 4205; 4249	100	Yes	Yes
S	G1085R	G24815A	4055; 4204; 4205; 4249	100	Yes	No
S	T1117I	C24912T	4249	35.0	No	Yes
ORF3a	T12I	C25427T	4205	99.9	Yes	Yes
ORF3a	S26L	C25469T	4055; 4204; 4205; 4249	100	Yes	Yes
ORF3a	R134H	G25793A	4055; 4205; 4249	100	Yes	No
M	I82T	T26767C	4055; 4204; 4205; 4249	100	Yes	Yes

(*Continued on next page*)

Table 3. *Continued*

Gene	Amino Acid Mutation	Nucleotide Mutation	Nasal Swab ID(s)	Max Allele Fraction (%)[a]	Major Variant?[b]	Found in other white-tailed deer SARS-CoV-2 sequences[c]
ORF7a	T39I	C27509T	4204; 4205	100	Yes	Yes
ORF7a	V82A	T27638C	4055; 4205; 4249	100	Yes	Yes
ORF7a	T120I	C27752T	4055; 4205; 4249	100	Yes	Yes
ORF8	S43F	C28021T	4249	29.9	No	Yes
ORF8	L60F, Δ61-66	TGTGCGTGGATGAGGCTGG28072T	4205	59.3	No	No
ORF8	L60F	G28073T	4055; 4249	100	Yes	Yes
ORF8	S67*, ΔK68	TCTA28092T	4205	95.6	Yes	No
ORF8	ΔDF119-120	AGATTTC28247A	4055; 4205; 4249	87.2	Yes	Yes
ORF8	F120L	C28253A	4055; 4249	100	Yes	No
N	D63G	A28461G	4055; 4204; 4205; 4249	100	Yes	Yes
N	R203M	G28881T	4055; 4204; 4205; 4249	100	Yes	Yes
N	G215C	G28916T	4055; 4204; 4205; 4249	100	Yes	Yes
N	D377Y	G29402T	4055; 4204; 4205; 4249	100	Yes	Yes

[a]The maximum allele fraction for each variant observed in all sequenced samples was calculated from the number of alternate allele observations divided by the total number of observations for each variant site.
[b]A variant with an allele fraction of at least 0.75 or 75% was classified as a major variant.
[c]As of 2023-08-28.

downregulated are associated with microtubules (e.g., *dynein cytoplasmic 2 heavy chain 1* [*DYNC2H1*], *dynein light chain roadblock-type 2* [*DYNLRB2*], *dynein axonemal heavy chain 3* [*DNAH3*], *DNAH5, DNAH7*) that make up extracellular structures such as cilia, likely reflecting host epithelial damage.

Comparison of white-tailed deer and human host response to SARS-CoV-2 infection

To identify potential differences in SARS-CoV-2 host responses between humans and WTD, we compared the $\log_2$ fold change of SARS-CoV-2 positive samples to negative samples from human and WTD nasopharyngeal swabs (Figure 5A and Table S8). The human cohort included 50 SARS-CoV-2 positive patients with a range of disease severity (18 admitted to the intensive care unit [ICU], 16 hospitalized, non-ICU, and 16 outpatients) and 13 SARS-CoV-2 negative individuals.[25] The coverage of gene detection in the WTD samples was comparable to that of the human cohort; 67.10% of genes detected ±5.48% (57.93–72.85%) out of a total of 26,670 genes in the WTD reference and the human nasopharyngeal samples had 63.57% of genes detected ±4.53% (54.47–74.43%). When examining all genes associated with innate immune response, there is a weak but statistically significant correlation between WTD and human nasopharyngeal $\log_2$ fold change ($r = 0.27$, p value = $9.49\text{x}10^{-13}$), with a slightly higher correlation observed when comparing against only outpatients ($r = 0.35$, p value = $1.45\text{x}10^{-20}$). For this analysis we only focused on the ~81% of WTD genes with detected human orthologs and did not include WTD-specific DEGs. We identified several immune-related genes that were significantly up-regulated in WTD and not in the human clinical cohort, including *IFNλ1*, *BST2*, and *IFITM1* (Figure 5B). In the data from the Butler and colleagues[26] human clinical cohort (RNAseq of naso/oropharyngeal swabs collected from 669 patients), some of these genes are significantly differentially expressed in SARS-CoV-2 positive versus negative patients, but still had low $\log_2$ fold changes when compared to WTD (0.84, 1.93, and 1.94 respectively), although the expression levels of these genes generally increased when comparing patients with higher viral loads than those with none.[26] Key viral entry and attachment factors for human SARS-CoV-2 infection were also examined in this way (Figure S5), with five of the set (*ACE2*, *basigin* [*BSG*], *cathepsin V* [*CTSV*], *metalloproteinase 2* [*MMP2*], and *SIGLEC1*) being significant DEGs in the human nasopharyngeal samples compared to only one (*SIGLEC1*) in the WTD samples.

Orthology analysis between human and the *texanus* subspecies of WTD revealed two interferon induced transmembrane 1 (*IFITM1*) genes in WTD, compared to a single copy in humans. Both genes were significantly over-expressed in WTD with SARS-CoV-2 infections ($\log_2$ fold change of 4.84 and 5.42 with adjusted p values of $2.82\text{x}10^{-8}$ and $1.53\text{x}10^{-13}$ for *LOC110149600* and *LOC110149612*, respectively). However, in the human cohort, *IFITM1* was not significantly differentially expressed, and $\log_2$ fold change values were low. Other WTD genomes (strains 20LAN1187 and brownington 1) were also confirmed to have two *IFITM1* genes, with 99% similarity between the sequenced *LOC110149600* genes (2–4 nucleotide differences) and 99% similarity between the *LOC110149612* genes (6–12 nucleotide differences). *LOC110149600* and *LOC110149612* are separated on the genome, with an average distance of 26,485 ± 486 base pairs apart. The *LOC110149612* transcript has an extended N-terminus compared to *LOC110149600* but with respect to their protein sequences, there are only three amino acid substitutions between them: valine/methionine (position 10), leucine/methionine (position 11), and valine/methionine (position 20) for *LOC110149612* and *LOC110149600*, respectively. Near identical IFITM1 sequences were also found in the other two WTD genomes. The identity between the

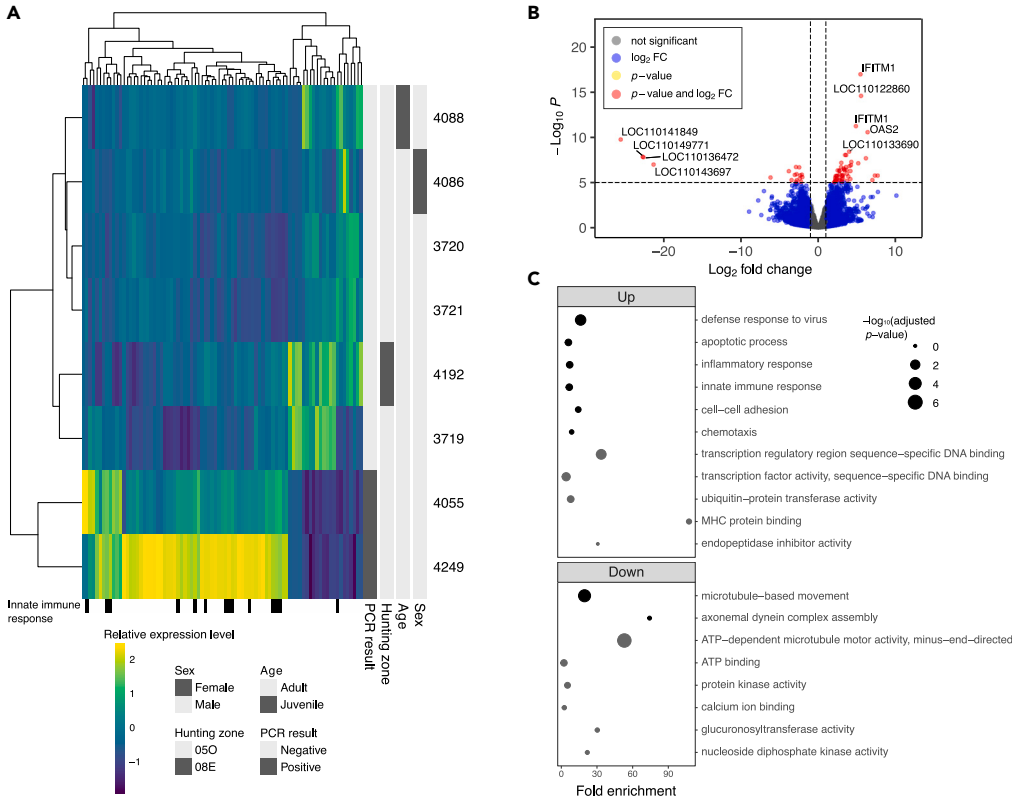

Figure 4. RNAseq analysis of white-tailed deer (WTD) nasopharyngeal swabs comparing uninfected WTD with SARS-CoV-2 infected WTD (4055 and 4249)

(A) Relative expression levels of significant (adjusted p value <0.05) differentially expressed genes with an absolute fold change greater than 3. WTD genes with human orthologs annotated with the Gene Ontology "innate immune response" term indicated underneath.

(B) Volcano plot of the DESeq2 differential gene expression analysis results. Where possible, genes were labeled with their inferred human ortholog gene name. The upper *interferon induced transmembrane protein 1* (*IFITM1*) is associated with *LOC110149600* and the lower *IFITM1* is associated with *LOC110149612* in the WTD genome.

(C) Gene Ontology function enrichment of the significant up and down-differentially expressed genes against a WTD genome background with DAVID. Only terms from biological processes (black dots) and molecular functions (gray dots) are displayed. See also Figures S3 and S4 and Tables S3, S4, S5, S6, and S7.

human and WTD IFITM1 proteins was much lower at 66–68%, with differences in the N-terminus including several unique proline substitutions that could impact protein structure. A Fixed Effects Likelihood analysis identified positions 20, 113, and 115 to have evidence of diversifying selection (Table S9), with all three of these positions differing between humans and WTD. A phylogenetic tree based on IFITM1 proteins from boreoeutherian mammals shows multiple instances of *IFITM1* gene duplication, all showing the extensive diversification *IFITM1* has undergone throughout mammals and the substantial differences between human and WTD IFITM1 (Figure 6).

DISCUSSION

In this report, we detected SARS-CoV-2 in 1.6% (95% CI 0.5–4.2%) of nasal swabs from sampled WTD in the Estrie region of southern Québec; viral sequences were assigned to lineage AY.44, a sublineage of the Delta variant of concern (VOC). Delta was the predominant circulating VOC at the time these animals were sampled. However, several unique mutations observed in the WTD sequences were not observed in the closely related AY.44 sequences from GISAID, supporting sustained deer-deer transmission. The WTD derived sequences from this study were most closely related to SARS-CoV-2 sequences from humans in neighboring Vermont, USA and one sequence from a human in Québec (Figure 2). Although we included SARS-CoV-2 sequences from humans from Québec in the analysis, it is unknown if any of these sequences were from the Estrie region. When compared to other deer derived SARS-CoV-2 sequences, the WTD SARS-CoV-2 sequences from this study were most closely related to sequences from north-eastern USA (Figure 3). While the Estrie region borders Vermont, to our knowledge, there is no evidence of SARS-CoV-2 in WTD or other wildlife species in Vermont reported to date.[27]

Whole SARS-CoV-2 genome sequences were found to contain two S gene mutations (S:T22I and S:A27V) that were different between WTD SARS-CoV-2 and the most closely related AY.44 sequences from GISAID. These changes are both located in the N terminal domain (NTD) of S1, which harbors antigenic and glycan-binding sites, and may interact with auxiliary receptors.[28] Changes at amino acid position 22 and 27

Table 4. Top 10 up and down differentially expressed white-tailed deer genes ranked by adjusted p value

Log_2 fold change	Adjusted p value	WTD gene name	Inferred human ortholog[a]
Up			
5.42	$1.49x10^{-13}$	interferon-induced transmembrane protein 1-like (*LOC110149612*)	*IFITM1*
5.50	$1.84x10^{-11}$	interferon alpha-inducible protein 27-like protein 2A (*LOC110122860*)	
4.84	$2.75x10^{-8}$	interferon-induced transmembrane protein 1-like (*LOC110149600*)	*IFITM1*
6.34	$9.71x10^{-8}$	2′-5′-oligoadenylate synthetase 2 (*OAS2*)	
3.96	$9.12x10^{-6}$	pleckstrin homology domain-containing family A member 4-like (*LOC110133690*)	
3.57	$1.66x10^{-5}$	hematopoietic SH2 domain containing (*HSH2D*)	*HSH2D*
3.44	$1.66x10^{-5}$	DNA dC- > dU-editing enzyme APOBEC-3H-like (*LOC110129971*)	*APOBEC3H*
6.12	$2.70x10^{-5}$	zonadhesin (*ZAN*)	*ZAN*
4.24	$6.32x10^{-5}$	complement C4-A-like (*LOC110139391*)	*C4B_2*
2.95	$7.22x10^{-5}$	transporter 1, ATP binding cassette subfamily B member (*TAP1*)	*TAP1*
Down			
−25.49	$5.00x10^{-7}$	heterogeneous nuclear ribonucleoprotein A1-like (*LOC110141849*)	
−22.66	$2.23x10^{-5}$	cuticlin-2-like (*LOC110149771*)	
−22.56	$2.31x10^{-5}$	ornithine decarboxylase antizyme 1-like (*LOC110136472*)	
−21.26	$9.82x10^{-5}$	heterogeneous nuclear ribonucleoprotein A1-like (*LOC110143697*)	
−2.90	$1.42x10^{-4}$	testis expressed 9 (*TEX9*)	*TEX9*
−2.48	$1.43x10^{-4}$	G protein subunit alpha 14 (*GNA14*)	*GNA11*
−3.82	$2.68x10^{-4}$	janus kinase and microtubule interacting protein 2 (*JAKMIP2*)	*JAKMIP2*
−2.82	$5.32x10^{-4}$	coiled-coil domain containing 181 (*CCDC181*)	*CCDC181*
−2.14	$5.68x10^{-4}$	homer scaffold protein 2 (*HOMER2*)	*HOMER2*
−3.04	$5.68x10^{-4}$	histamine receptor H1 (*HRH1*)	*HRH1*

See also Tables S3–S7.

[a]If left blank, no human ortholog could be predicted with OrthoFinder.

have been noted early in the pandemic, with up to four different amino acid variants at position 27; this plasticity is suggestive of an adaptive evolutionary role.[29,30] We have since detected the S:T22I mutation in a highly divergent, WTD-adapted SARS-CoV-2 from Ontario,[10] further supporting a relevant role for changes in this region of the S protein. Additionally, in one WTD (4205), two inframe deletions in ORF8 were observed. The ORF8 gene is hypervariable and encodes for a non-essential accessory protein and has been shown to downregulate the major histocompatibility complex class I through autophagic degradation, thus impairing cytotoxic T cell responses during SARS-CoV-2, but not SARS-CoV infection.[31] It may also contribute to immune evasion through interferon antagonism.[32,33] More recently, ORF8 protein was found to purportedly mimic host interleukin-17 that contributes to severe inflammation in COVID-19.[34] Truncation of ORF8 arising from nonsense mutations and deletions have been previously observed in both human and animal derived sarbecoviruses (SARS-CoV and SARS-CoV-2)[32,35–37] and may be associated with milder disease through enhanced T cell functions. This underscores the potential role of ORF8 in SARS-CoV-2 adaptation.

All RT-PCR-positive WTD were identified in the Estrie region (Table 1; Figure 1). While it is presently unclear how the WTD acquired SARS-CoV-2 infection, there are several notable differences between the sampled regions that may contribute to the spatial heterogeneity of infection: 1) WTD population density and hunter harvest are greater in Estrie (13–15 WTD/km^2) compared to the Laurentides (~1 WTD/km^2) (MELCCFP, unpublished data), 2) the sampled regions in Estrie have higher human population density compared to sampled regions in the Laurentides (Figure 1A), and 3) COVID-19 positivity in humans was greater in Estrie (4.2%) during the study period compared to the Laurentides (2.3%).[38] Although the spatial clustering of SARS-CoV-2 in WTD has been previously reported in other regions,[1,5,6] it is possible that the identification of SARS-CoV-2 in WTD only in the Estrie region could be a result of temporally and geographically limited sampling. More longitudinal surveillance of SARS-CoV-2 in WTD is needed to understand the epidemiology of the virus in this species and how it relates to

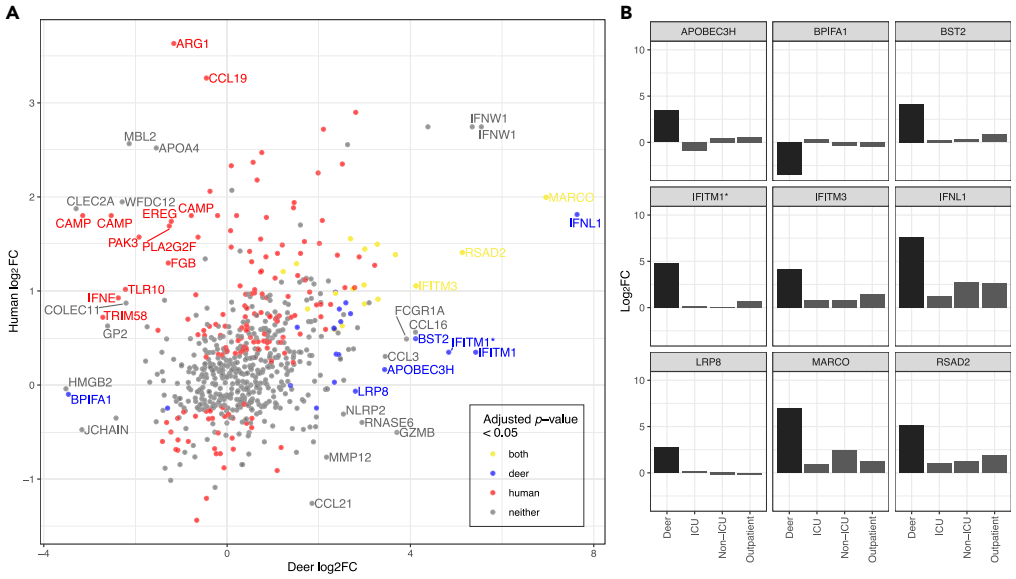

Figure 5. Comparison of the white-tailed deer (WTD) versus human host response to SARS-CoV-2 infection

(A) The WTD expression fold change is plotted here against the human expression fold change from comparable human samples based on the results of an orthology analysis between WTD and human. The genes are labeled with the respective human gene name, if the absolute difference in $\log_2$ fold change values between the human and WTD expression profiles is greater than 2.5. Due to duplicated genes in the WTD genome, some points are labeled with the same human gene name. From left to right, *cathelicidin antimicrobial peptide* (*CAMP*) genes are associated with *LOC110152352*, *LOC110152353*, and *LOC110152344* in the WTD genome, *interferon omega 1* (*IFNω1*) genes are associated with *LOC110144825* and *LOC110144833* and *interferon induced transmembrane protein 1* (*IFITM1*) genes are associated with *LOC110149600* and *LOC110149612*. Points are colored based on significance in their respective differentially gene expression analysis. Genes with very low expression values are not given a p value in the DESeq2 analysis and are not considered significant. (B) Genes that are significantly differentially expressed in the WTD SARS-CoV-2 infection and have an absolute difference in $\log_2$ fold change values between the human and WTD infections greater than 2.5 are plotted here with their corresponding $\log_2$ fold change values across different levels of human disease severity. Intensive care unit (ICU), non-ICU, and outpatient are comparisons of human nasopharyngeal swabs between patients from these respective settings, and healthy patients. Genes are labeled with their human ortholog gene name. *IFITM1* here corresponds to *LOC110149600* in the WTD genome. See also Table S8.

WTD ecology and transmission dynamics in sympatric humans. These are important considerations for understanding the potential role of WTD as a maintenance population or reservoir for SARS-CoV-2.

Experimental data demonstrate that productive viral replication is limited to the upper respiratory tract with the shedding of infectious virus in nasal secretions of infected WTD.[3,9] We successfully isolated viable SARS-CoV-2 from two RT-PCR-positive nasal swabs, demonstrating viral infectivity. This suggests there is a potential risk of contact with infectious SARS-CoV-2 from WTD, and several probable deer-to-human transmission events have been reported to date.[10,12] These findings warrant increased awareness of the risks associated with direct human contact with live free-living and captive WTD and their carcasses.[39]

Work characterizing the WTD host response to SARS-CoV-2 infection is limited. Our study is the first to explore the host response in WTD naturally infected with SARS-CoV-2. Davila and colleagues conducted a comparative transcriptomics analysis of SARS-CoV-2 infected human and WTD primary respiratory tracheal epithelial cells *in vitro*, finding evidence of differing early innate immune responses.[40] Compared to the work by Davila and colleagues,[41] there is no overlap in significant DEGs observed in our study. This may be because of the difference in the anatomical site (e.g., nasal cavity vs. trachea) of sampling and differences between *in vitro* and *in vivo* systems (e.g., the absence of commensal flora in the former). Additionally, the course of infection for WTD in the present study is unknown and may not be comparable to infection time points for the tracheal cells derived from experimentally infected cells, as well as differences attributable to responses elicited by ancestral SARS-CoV-2 vs. the Delta VOC. Indeed, our data suggest the need for controlled *in vivo* studies in WTD to map differential host responses upon SARS-CoV-2 infection and delineate the pathological outcomes of infection in this ecologically important mammalian species.

Host expression patterns in SARS-CoV-2 infected WTD were associated with the innate immune response, including signaling pathways related to anti-viral and pro-inflammatory signaling and host damage. There was evidence for type I and III IFN responses (e.g., *IRF3, IRF4, IRF5, IRF7, IRF9, INFλ3, STAT2, IFITM1, IFITM2, IFITM3, IFI6, IFI27L2A*). The type I IFN response is an important aspect of rapidly controlling viral infection, and dysregulation is associated with severe illness and pathology. Type III IFNs produce a more localized response to infection in comparison to the systemic inflammatory response often induced by type I IFN; type III IFNs also result in prolonged expression of ISGs.[42] Upregulation of pro-inflammatory antagonists were also observed. For example, there was increased expression of transcripts for two nuclear factor kappa-light-chain-enhancer of activated B cells (NF-KB) inhibitors (e.g., *NFKB inhibitor delta* [*NFKBID*], *NFKB inhibitor zeta* [*NFKBIZ*]) which could indicate a mechanism to reduce immunopathology or indicate a switch toward the resolution of inflammation (e.g., tissue repair).[43] Additionally, several genes involved in antiviral response and inflammation homeostasis were found to have multiple transcript

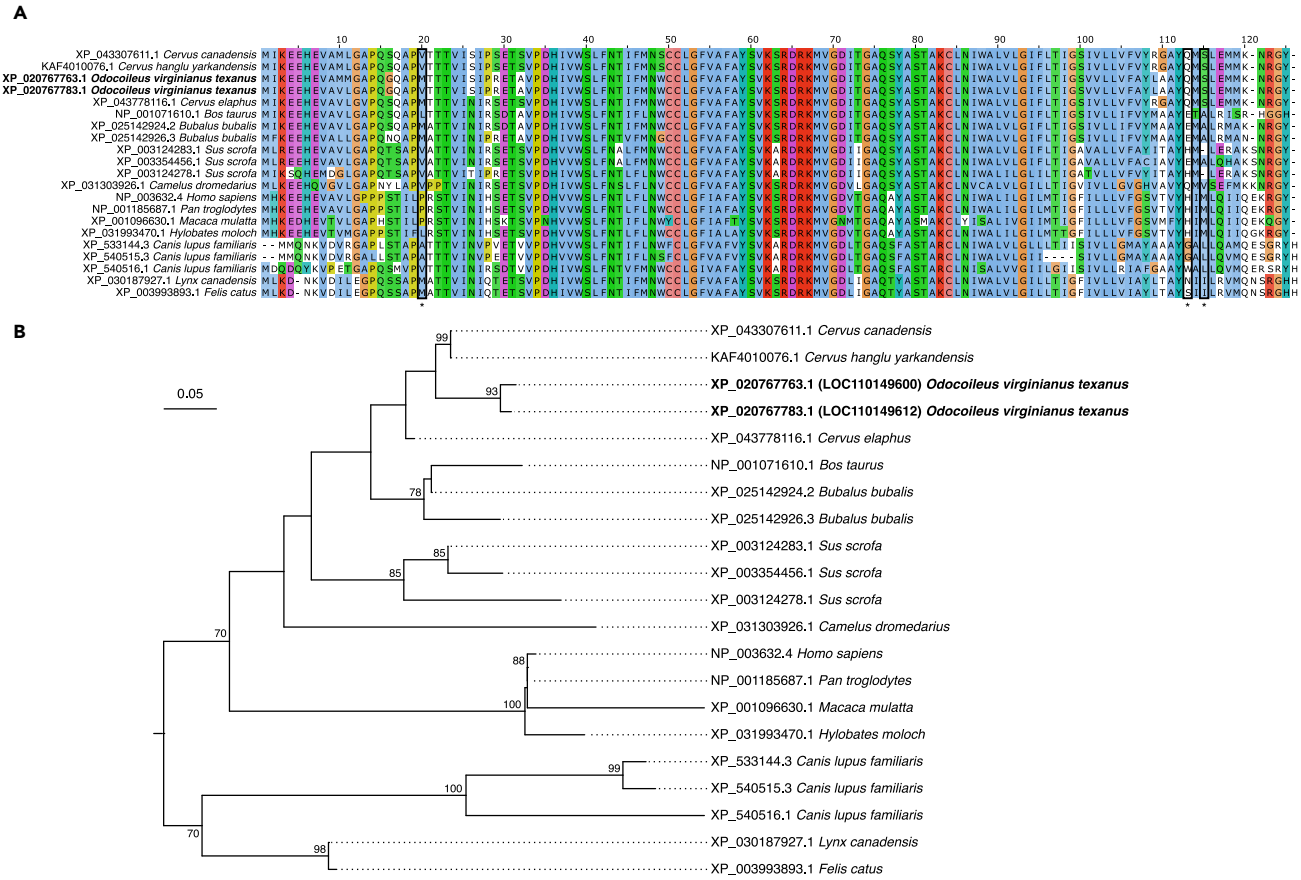

Figure 6. Phylogenetic analysis of interferon induced transmembrane protein 1 (IFITM1) in mammals reveals lineage-specific duplications in white-tailed deer and evolutionary diversification

(A) Alignment of IFITM1 from select boreoeutherian mammals. An extended N-terminal start to XP_043307611.1 (*Cervus canadensis*) and XP_025142924.2 (*Bubalus bubalis*) has been trimmed from the alignment. Boxed and asterisked positions 20, 113 and 115 were identified as sites of diversifying selection. Alignment is colored with the Clustal color scheme with poorly conserved residues left white using Jalview v2.11.2.6.

(B) A mid-point rooted tree of IFITM1 from select boreoeutherian mammals. Bootstrap values less than 70 were not displayed. See also Table S9.

variants (e.g., *IFITM1*, *XAF1*) which may also contribute to protecting the host from inflammation.[44,45] Nothing is known about antiviral gene duplication in WTD and their role in antiviral immune response.

When examining all genes associated with innate immune response, there was a weak but statistically significant correlation between WTD and human $\log_2$ fold change, with the strongest correlation observed between WTD and outpatients. Previous studies have reported that WTD infected with SARS-CoV-2 do not present with overt signs of infection or pathology; only minor pathological changes associated with rhinitis and loss of cilia in the respiratory epithelium have been observed in experimentally infected WTD.[3,7,9] However, the duration of infection for each individual host in our study was unknown, limiting the inferences that can be made regarding the dynamics of innate immune responses. Additionally, it is unclear whether infection with SARS-CoV-2 results in any sublethal effects (e.g., body condition, winter survival, reproduction) despite no overt signs of disease.

There were also DEGs with substantial differences within the innate immune response gene set, notably *macrophage receptor with collagenous structure* (*MARCO*), *IFNL1*, *IFITM1*, *IFITM3*, *radical s-adenosyl methionine domain containing 2* (*RSAD2*), *BST2*, *APOBEC3H*, *low-density lipoprotein receptor-related protein 8* (*LRP8*), and *BPI fold containing family A member 1* (*BPIFA1*). These genes had a large difference (>2.5) in $\log_2$ fold change values between the human and WTD DEGs while also being significantly differentially expressed in the WTD samples. These data indicate that the WTD nasal epithelium expressed genes that encode antiviral proteins, including the *IFITM* family, in response to SARS-CoV-2 infection. IFITMs are membrane proteins that restrict viral entry for a broad spectrum of enveloped viruses.[46,47] In contrast, studies in human cells have shown that SARS-CoV-2 has been shown to hijack IFITMs for efficient cellular entry, a process mediated by specific interactions between the N-terminal region of IFITMs and the viral S protein.[45,47] Intriguingly, *IFITM1* has undergone a lineage-specific duplication resulting in two copies in WTD and transcripts for both were significantly upregulated in our samples. The amino acid changes between the two WTD IFITM1 are present in other mammalian (e.g., other deer in the *Cervus* genus and Felinae) lineages and are thus not unique to WTD, but the mutations appear to have evolved independently on several occasions (Figure 6). More importantly,

the N- and C-terminal ends of both IFITM1 possess unique differences in WTD compared to human IFITM1. We speculate that these differences might contribute to differences in antiviral properties or efficiency of IFITM1 activity in WTD (and other animals) versus humans, as previously seen with the IFITM3 family in primates,[48] and are an important future target for characterizing SARS-CoV-2-WTD molecular interactions.

Surveillance for SARS-CoV-2 in wildlife is ongoing across Canada. Our findings underscore that longitudinal surveillance efforts in WTD in Québec and across Canada are warranted. We provide preliminary insights into unique transcriptional responses in WTD that are naturally infected with SARS-CoV-2. Further work is needed to understand the mechanisms that facilitate virus transmission from humans to deer and among WTD, along with identifying selection pressures within WTD that promote adaptive mutations within the viral genome. Additionally, more longitudinal epidemiological and ecological data is needed to better understand whether WTD truly represent a competent maintenance population or reservoir for SARS-CoV-2. Ongoing coordinated and cross-disciplinary efforts are required to ensure a One Health approach is applied to this critical pandemic challenge by informing evidence-based decision-making for human and animal health.

Limitations of the study

While leveraging annual WTD hunting season resulted in many samples, the present work was conducted over a short time and a relatively small geographic region. Therefore, our study represents a snapshot in time and space. Future work should aim to obtain longitudinal data to investigate maintenance of SARS-CoV-2 in Québec WTD populations and assess spatiotemporal patterns in pathogen ecology. Samples analyzed in this study were derived from harvested WTD and were therefore collected postmortem. Although 98% of samples were collected within 48 h of harvest, it is possible that inhibitors or sample degradation occurred between harvest and sample collection. The low prevalence and available sample material for follow-up analysis resulted in a low sample size of SARS-CoV-2 positive WTD for the transcriptomic analysis. Finally, our study only focuses on free-ranging WTD populations, and we therefore cannot make inferences about SARS-CoV-2 in captive conspecifics.

STAR★METHODS

Detailed methods are provided in the online version of this paper and include the following:

- KEY RESOURCES TABLE
- RESOURCE AVAILABILITY
  - Lead contact
  - Materials availability
  - Data and code availability
- EXPERIMENTAL MODEL AND SUBJECT DETAILS
  - Ethical statement
  - Sample collection and study region
  - Cells lines
- METHOD DETAILS
  - Biosafety
  - RT-PCR screening and detection
  - SARS-CoV-2 amplification and sequencing
  - Virus isolation
  - RNA-sequencing of white-tailed deer nasal swabs
  - RNA-seq bioinformatic analysis of white-tailed deer nasal swabs
  - IFITM1 comparison within O. virginianus and mammalian IFITM1 phylogenetics
- QUANTIFICATION AND STATISTICAL ANALYSIS

SUPPLEMENTAL INFORMATION

Supplemental information can be found online at https://doi.org/10.1016/j.isci.2023.108319.

ACKNOWLEDGMENTS

We thank the hunters for the deer submissions. Many thanks to the technicians and biologists who assisted with sample collection (Matthew Rokas-Bérubé, Yannicia Fréchette-Hudon, Catherine Greaves, Charles-Étienne Gagnon, Marylou Meyer, Camille Klein, Stéphane Lamoureux, Yannick Bilodeau, François Lebel, Sophie Plante, and Isabelle Laurion), the technicians that assisted with sample analysis (Emily Chien, Mathieu Pinette, Winfield Yim, Melissa Goolia, and Nikki Toledo), and Michelle Nebroski who assisted with sequencing data analysis. We are grateful for the work of D. Bulir in developing the UTR gene target used in the Sunnybrook Research Institute RT-PCR analysis. The graphical abstract for this article was prepared with BioRender.com.

This work was supported by the Public Health Agency of Canada, and Canadian Institutes of Health Research Operating Grant: Emerging COVID-19 Research Gaps and Priorities (466984). J.D.K. is supported by an AMMI Canada/BioMérieux Fellowship in Microbial Diagnostics. Funding and computing resources for F.M were provided by the Shared Hospital Laboratory, Dalhousie University, and the Donald Hill Family.

O.L. was supported by the Canadian Safety and Security Program, Laboratories Canada, and Canadian Food Inspection Agency (CFIA) Genomics Development and Research Initiative. A.B. also acknowledges support from Natural Sciences and Engineering Research Council of Canada (NSERC), Canadian Institutes of Health Research (CIHR), and Coronavirus Variants Rapid Response Network (CoVaRR-Net). VIDO receives operational funding for its CL3 facility (InterVac) from the Canada Foundation for Innovation through the Major Science Initiatives. VIDO also receives operational funding from the Government of Saskatchewan through Innovation Saskatchewan and the Saskatchewan Ministry of Agriculture.

AUTHOR CONTRIBUTIONS

Conceptualization: J.D.K., A.M., M.G., J.B., T.B., B.P., and S.M.

Sample collection: J.D.K., A.M., and M.G.

Laboratory analysis: J.D.K, P.A., J.B.S., H.Y.C., K.N., L.Y., L.R.L., and B.P.

Data analysis/Investigation: J.D.K., B.L., P.K., F.M., O.V., and O.L.

Writing – original draft: J.D.K., and B.L.

Writing – review & editing: All authors.

Visualization: J.D.K., B.L., P.K., A.C.D., O.V., and O.L.

Supervision: L.R.L., A.C.D., O.L., B.P., and S.M.

Funding acquisition: A.M., M.G., and S.M.

Co-corresponding authors are justified from One Health and multidisciplinary perspectives: B.P. (animal health perspective and reference laboratory, confirmatory testing and reporting to the World Organization for Animal Health); A.D. (RNAseq computational biology); S.M. (human health perspective and initial virus detection, sequencing, isolation and generation of RNAseq dataset; lead contact).

DECLARATION OF INTERESTS

The authors declare no conflicts relevant to this article.

INCLUSION AND DIVERSITY

We support inclusive, diverse, and equitable conduct of research.

Received: June 16, 2023
Revised: September 12, 2023
Accepted: October 20, 2023
Published: October 24, 2023

REFERENCES

1. Caserta, L.C., Martins, M., Butt, S.L., Hollingshead, N.A., Covaleda, L.M., Ahmed, S., Everts, M.R.R., Schuler, K.L., and Diel, D.G. (2023). White-tailed deer (*Odocoileus virginianus*) may serve as a wildlife reservoir for nearly extinct SARS-CoV-2 variants of concern. Proc. Natl. Acad. Sci. USA *120*, e2215067120. https://doi.org/10.1073/pnas.2215067120.
2. Chandler, J.C., Bevins, S.N., Ellis, J.W., Linder, T.J., Tell, R.M., Jenkins-Moore, M., Root, J.J., Lenoch, J.B., Robbe-Austerman, S., DeLiberto, T.J., et al. (2021). SARS-CoV-2 exposure in wild white-tailed deer (*Odocoileus virginianus*). Proc. Natl. Acad. Sci. USA *118*, e2114828118. https://doi.org/10.1073/pnas.2114828118.
3. Cool, K., Gaudreault, N.N., Morozov, I., Trujillo, J.D., Meekins, D.A., McDowell, C., Carossino, M., Bold, D., Mitzel, D., Kwon, T., et al. (2022). Infection and transmission of ancestral SARS-CoV-2 and its alpha variant in pregnant white-tailed deer. Emerg. Microbes Infect. *11*, 95–112. https://doi.org/10.1080/22221751.2021.2012528.
4. Hale, V.L., Dennis, P.M., McBride, D.S., Nolting, J.M., Madden, C., Huey, D., Ehrlich, M., Grieser, J., Winston, J., Lombardi, D., et al. (2022). SARS-CoV-2 infection in free-ranging white-tailed deer. Nature *602*, 481–486. https://doi.org/10.1038/s41586-021-04353-x.
5. Kuchipudi, S.V., Surendran-Nair, M., Ruden, R.M., Yon, M., Nissly, R.H., Vandegrift, K.J., Nelli, R.K., Li, L., Jayarao, B.M., Maranas, C.D., et al. (2022). Multiple spillovers from humans and onward transmission of SARS-CoV-2 in white-tailed deer. Proc. Natl. Acad. Sci. USA *119*, e2121644119. https://doi.org/10.1073/pnas.2121644119.
6. Marques, A.D., Sherrill-Mix, S., Everett, J.K., Adhikari, H., Reddy, S., Ellis, J.C., Zeliff, H., Greening, S.S., Cannuscio, C.C., Strelau, K.M., et al. (2022). Multiple Introductions of SARS-CoV-2 Alpha and Delta Variants into White-Tailed Deer in Pennsylvania. mBio *13*, e0210122. https://doi.org/10.1128/mbio.02101-22.
7. Martins, M., Boggiatto, P.M., Buckley, A., Cassmann, E.D., Falkenberg, S., Caserta, L.C., Fernandes, M.H.V., Kanipe, C., Lager, K., Palmer, M.V., and Diel, D.G. (2022). From Deer-to-Deer: SARS-CoV-2 is efficiently transmitted and presents broad tissue tropism and replication sites in white-tailed deer. PLoS Pathog. *18*, e1010197. https://doi.org/10.1371/journal.ppat.1010197.
8. Palermo, P.M., Orbegozo, J., Watts, D.M., and Morrill, J.C. (2022). SARS-CoV-2 SARS-CoV-2 neutralizing antibodies in white-tailed deer from Texas. Vector Borne Zoonotic Dis. *22*, 62–64. https://doi.org/10.1089/vbz.2021.0094.
9. Palmer, M.V., Martins, M., Falkenberg, S., Buckley, A., Caserta, L.C., Mitchell, P.K., Cassmann, E.D., Rollins, A., Zylich, N.C., Renshaw, R.W., et al. (2021). Susceptibility of white-tailed deer (*Odocoileus virginianus*) to SARS-CoV-2. J. Virol. *95*, e00083-21. https://doi.org/10.1089/vbz.2021.0094.
10. Pickering, B., Lung, O., Maguire, F., Kruczkiewicz, P., Kotwa, J.D., Buchanan, T., Gagnier, M., Guthrie, J.L., Jardine, C.M., Marchand-Austin, A., et al. (2022). Divergent SARS-CoV-2 variant emerges in white-tailed deer with deer-to-human transmission. Nat. Microbiol. *7*, 2011–2024. https://doi.org/10.1038/s41564-022-01268-9.
11. Roundy, C.M., Nunez, C.M., Thomas, L.F., Auckland, L.D., Tang, W., Richison, J.J., Green, B.R., Hilton, C.D., Cherry, M.J., Pauvolid-Corrêa, A., et al. (2022). High seroprevalence of SARS-CoV-2 in white-tailed deer (*Odocoileus virginianus*) at one of three captive cervid facilities in Texas. Microbiol. Spectr. *10*, e0057622. https://doi.org/10.1128/spectrum.00576-22.
12. Feng, A., Bevins, S., Chandler, J., DeLiberto, T.J., Ghai, R., Lantz, K., Lenoch, J., Retchless, A., Shriner, S., Tang, C.Y., et al. (2023).

Transmission of SARS-CoV-2 in free-ranging white-tailed deer in the United States. Nat. Commun. *14*, 4078. https://doi.org/10.1038/s41467-023-39782-x.

13. McBride, D.S., Garushyants, S.K., Franks, J., Magee, A.F., Overend, S.H., Huey, D., Williams, A.M., Faith, S.A., Kandeil, A., Trifkovic, S., et al. (2023). Accelerated evolution of SARS-CoV-2 in free-ranging white-tailed deer. Res. Sq. rs.3.rs-2574993. https://doi.org/10.1038/s41467-023-40706-y.
14. Tan, C.C.S., Lam, S.D., Richard, D., Owen, C.J., Berchtold, D., Orengo, C., Nair, M.S., Kuchipudi, S.V., Kapur, V., van Dorp, L., and Balloux, F. (2022). Transmission of SARS-CoV-2 from humans to animals and potential host adaptation. Nat. Commun. *13*, 2988. https://doi.org/10.1038/s41467-022-30698-6.
15. Bashor, L., Gagne, R.B., Bosco-Lauth, A.M., Bowen, R.A., Stenglein, M., and VandeWoude, S. (2021). SARS-CoV-2 evolution in animals suggests mechanisms for rapid variant selection. Proc. Natl. Acad. Sci. USA *118*, e2105253118. https://doi.org/10.1073/pnas.2105253118.
16. Larsen, H.D., Fonager, J., Lomholt, F.K., Dalby, T., Benedetti, G., Kristensen, B., Urth, T.R., Rasmussen, M., Lassaunière, R., Rasmussen, T.B., et al. (2021). Preliminary report of an outbreak of SARS-CoV-2 in mink and mink farmers associated with community spread, Denmark, June to November 2020. Euro Surveill. *26*, 2100009. https://doi.org/10.2807/1560-7917.es.2021.26.5.210009.
17. Wei, C., Shan, K.-J., Wang, W., Zhang, S., Huan, Q., and Qian, W. (2021). Evidence for a mouse origin of the SARS-CoV-2 Omicron variant. J. Genet. Genom. *48*, 1111–1121. https://doi.org/10.1016/j.jgg.2021.12.003.
18. Becker, D.J., and Banerjee, A. (2023). Coupling field and laboratory studies of immunity and infection in zoonotic hosts. Lancet. Microbe *4*, E285–E287. https://doi.org/10.1016/S2666-5247(23)00032-0.
19. Mandl, J.N., Ahmed, R., Barreiro, L.B., Daszak, P., Epstein, J.H., Virgin, H.W., and Feinberg, M.B. (2015). Reservoir host immune responses to emerging zoonotic viruses. Cell *160*, 20–35. https://doi.org/10.1016/S2666-5247(23)00032-0.
20. Ministère de l'Environnement, de la Lutte contre les changements and climatiques, de la Faune et des Parcs (2021). Chronic Wasting Disease in Cervids Surveillance and Control Operations.
21. World Organization for Animal Health (2021). SARS-CoV-2 in Animals – Situation Report 8. https://www.oie.int/app/uploads/2022/01/sars-cov-2-situation-report-8.pdf.
22. Naderi, S., Chen, P.E., Murall, C.L., Poujol, R., Kraemer, S., Pickering, B.S., Sagan, S.M., and Shapiro, B.J. (2023). Zooanthroponotic transmission of SARS-CoV-2 and host-specific viral mutations revealed by genome-wide phylogenetic analysis. Elife *12*, e83685. https://doi.org/10.7554/elife.83685.
23. Chen, Y., Liu, M.-Q., Luo, Y., Jiang, R.-D., Si, H.-R., Zhu, Y., Li, B., Shen, X.-R., Lin, H.-F., Zhao, K., et al. (2021). Genetic Mutation of SARS-CoV-2 during Consecutive Passages in Permissive Cells. Virol. Sin. *36*, 1073–1076. https://doi.org/10.1007/2Fs12250-021-00384-w.
24. Aiewsakun, P., Phumiphanjarphak, W., Ludowyke, N., Purwono, P.B., Manopwisedjaroen, S., Srisaowakarn, C., Ekronarongchai, S., Suksatu, A., Yuvaniyama, J., and Thitithanyanont, A. (2023). Systematic exploration of SARS-CoV-2 adaptation to Vero E6, Vero E6/TMPRSS2, and Calu-3 Cells. Genome Biol. Evol. *15*, evad035. https://doi.org/10.1093/gbe/evad035.
25. Luc, J., Lobb, B., Hirota, J., McGeer, A., Mubareka, S., and Doxey, A. (2023). Comparative Transcriptomic Analysis of Nasopharyngeal Swabs from Individuals with and without COVID-19 (Figshare). https://doi.org/10.6084/m9.figshare.22704403.v1.
26. Butler, D., Mozsary, C., Meydan, C., Foox, J., Rosiene, J., Shaiber, A., Danko, D., Afshinnekoo, E., MacKay, M., Sedlazeck, F.J., et al. (2021). Shotgun transcriptome, spatial omics, and isothermal profiling of SARS-CoV-2 infection reveals unique host responses, viral diversification, and drug interactions. Nat. Commun. *12*, 1660. https://doi.org/10.1038/s41467-021-21361-7.
27. Despres, H.W., Mills, M.G., Schmidt, M.M., Gov, J., Perez, Y., Jindrich, M., Crawford, A.M.L., Kohl, W.T., Rosenblatt, E., Kubinski, H.C., et al. (2023). Surveillance of Vermont wildlife in 2021-2022 reveals no detected SARS-CoV-2 viral RNA. Sci. Rep. *13*, 14683. https://doi.org/10.1038/s41598-023-39232-0.
28. Harvey, W.T., Carabelli, A.M., Jackson, B., Gupta, R.K., Thomson, E.C., Harrison, E.M., Ludden, C., Reeve, R., Rambaut, A., COVID-19 Genomics UK COG-UK Consortium, et al.. (2021). SARS-CoV-2 variants, spike mutations and immune escape. Nat. Rev. Microbiol. *19*, 409–424. https://doi.org/10.1038/s41579-021-00573-0.
29. Long, S.W., Olsen, R.J., Christensen, P.A., Bernard, D.W., Davis, J.J., Shukla, M., Nguyen, M., Saavedra, M.O., Yerramilli, P., Pruitt, L., et al. (2020). Molecular architecture of early dissemination and massive second wave of the SARS-CoV-2 virus in a major metropolitan area. mBio *11*, e02707-20. https://doi.org/10.1128/mbio.02707-20.
30. Saputri, D.S., Li, S., van Eerden, F.J., Rozewicki, J., Xu, Z., Ismanto, H.S., Davila, A., Teraguchi, S., Katoh, K., and Standley, D.M. (2020). Flexible, functional, and familiar: characteristics of SARS-CoV-2 spike protein evolution. Front. Microbiol. *11*. https://doi.org/10.3389/2Ffmicb.2020.02112.
31. Zhang, Y., Chen, Y., Li, Y., Huang, F., Luo, B., Yuan, Y., Xia, B., Ma, X., Yang, T., Yu, F., et al. (2021). The ORF8 protein of SARS-CoV-2 mediates immune evasion through down-regulating MHC-I. Proc. Natl. Acad. Sci. USA *118*, e2024202118. https://doi.org/10.1073/pnas.2024202118.
32. Li, J.-Y., Liao, C.-H., Wang, Q., Tan, Y.-J., Luo, R., Qiu, Y., and Ge, X.-Y. (2020). The ORF6, ORF8 and nucleocapsid proteins of SARS-CoV-2 inhibit type I interferon signaling pathway. Virus Res. *286*, 198074. https://doi.org/10.1016/j.virusres.2020.198074.
33. Moriyama, M., Lucas, C., Monteiro, V.S., and Iwasaki, A. (2022). SARS-CoV-2 variants do not evolve to promote further escape from MHC-I recognition. Preprint at bioRxiv. https://doi.org/10.1101/2022.05.04.490614.
34. Wu, X., Xia, T., Shin, W.-J., Yu, K.-M., Jung, W., Herrmann, A., Foo, S.-S., Chen, W., Zhang, P., Lee, J.-S., et al. (2022). Viral mimicry of interleukin-17A by SARS-CoV-2 ORF8. mBio *13*, e0040222. https://doi.org/10.1128/mbio.00402-22.
35. Fong, S.-W., Yeo, N.K.-W., Chan, Y.-H., Goh, Y.S., Amrun, S.N., Ang, N., Rajapakse, M.P., Lum, J., Foo, S., Lee, C.Y.-P., et al. (2022). Robust Virus-specific adaptive immunity in COVID-19 patients with SARS-CoV-2 Δ382 variant infection. J. Clin. Immunol. *42*, 214–229. https://doi.org/10.1007/s10875-021-01142-z.
36. Su, Y.C.F., Anderson, D.E., Young, B.E., Linster, M., Zhu, F., Jayakumar, J., Zhuang, Y., Kalimuddin, S., Low, J.G.H., Tan, C.W., et al. (2020). Discovery and genomic characterization of a 382-nucleotide deletion in ORF7b and ORF8 during the early evolution of SARS-CoV-2. mBio *11*, e01610-20. https://doi.org/10.1128/mbio.01610-20.
37. Young, B.E., Fong, S.-W., Chan, Y.-H., Mak, T.-M., Ang, L.W., Anderson, D.E., Lee, C.Y.-P., Amrun, S.N., Lee, B., Goh, Y.S., et al. (2020). Effects of a major deletion in the SARS-CoV-2 genome on the severity of infection and the inflammatory response: an observational cohort study. Lancet *396*, 603–611. https://doi.org/10.1016/S0140-6736(20)31757-8.
38. Institut national de and santé publique du Québec (INSPQ) (2021). Données COVID-19 Par Région Sociosanitaire (INSPQ). https://www.inspq.qc.ca/covid-19/donnees/par-region.
39. Public Health Agency of Canada (2021). Animals and COVID-19. https://www.canada.ca/en/public-health/services/diseases/2019-novel-coronavirus-infection/prevention-risks/animals-covid-19.html.
40. Davila, K.M.S., Nelli, R.K., Phadke, K.S., Ruden, R.M., Yongming, S., Bellaire, B.H., Gimenez-Lirola, L.G., and Miller, L.C. (2023). How do deer respiratory epithelial cells weather the initial storm of SARS-CoV-2?. Preprint at bioRxiv. https://doi.org/10.1101/2023.04.24.538130.
41. Yu, G., Smith, D.K., Zhu, H., Guan, Y., and Lam, T.T.-Y. (2017). ggtree: an r package for visualization and annotation of phylogenetic trees with their covariates and other associated data. Methods Ecol. Evol. *8*, 28–36. https://doi.org/10.1111/2041-210X.12628.
42. Broadbent, L., Bamford, C.G.G., Lopez Campos, G., Manzoor, S., Courtney, D., Ali, A., Touzelet, O., McCaughey, C., Mills, K., and Power, U.F. (2022). An endogenously activated antiviral state restricts SARS-CoV-2 infection in differentiated primary airway epithelial cells. PLoS One *17*, e0266412. https://doi.org/10.1371/journal.pone.0266412.
43. Lieberman, N.A.P., Peddu, V., Xie, H., Shrestha, L., Huang, M.-L., Mears, M.C., Cajimat, M.N., Bente, D.A., Shi, P.-Y., Bovier, F., et al. (2020). In vivo antiviral host transcriptional response to SARS-CoV-2 by viral load, sex, and age. PLoS Biol. *18*, e3000849. https://doi.org/10.1371/journal.pbio.3000849.
44. Han, Y., Bai, X., Liu, S., Zhu, J., Zhang, F., Xie, L., Liu, G., Jiang, X., Zhang, M., Huang, Y., et al. (2022). XAF1 Protects host against emerging RNA viruses by stabilizing IRF1-dependent antiviral immunity. J. Virol. *96*, e0077422. https://doi.org/10.1128/jvi.00774-22.
45. Shi, G., Kenney, A.D., Kudryashova, E., Zani, A., Zhang, L., Lai, K.K., Hall-Stoodley, L., Robinson, R.T., Kudryashov, D.S., Compton, A.A., and Yount, J.S. (2021). Opposing activities of IFITM proteins in SARS-CoV-2 infection. EMBO J. *40*, e106501. https://doi.org/10.15252/embj.2020106501.
46. Buchrieser, J., Dufloo, J., Hubert, M., Monel, B., Planas, D., Rajah, M.M., Planchais, C., Porrot, F., Guivel-Benhassine, F., Van der Werf, S., et al. (2020). Syncytia formation by SARS-CoV-2-infected cells. EMBO J. *39*,

e106267. https://doi.org/10.15252/embj.2020106267.

47. Prelli Bozzo, C., Nchioua, R., Volcic, M., Koepke, L., Krüger, J., Schütz, D., Heller, S., Stürzel, C.M., Kmiec, D., Conzelmann, C., et al. (2021). IFITM proteins promote SARS-CoV-2 infection and are targets for virus inhibition *in vitro*. Nat. Commun. *12*, 4584. https://doi.org/10.1038/s41467-021-24817-y.
48. Compton, A.A., Roy, N., Porrot, F., Billet, A., Casartelli, N., Yount, J.S., Liang, C., and Schwartz, O. (2016). Natural mutations in IFITM3 modulate post-translational regulation and toggle antiviral specificity. EMBO Rep. *17*, 1657–1671. https://doi.org/10.15252/embr.201642771.
49. LeBlanc, J.J., Gubbay, J.B., Li, Y., Needle, R., Arneson, S.R., Marcino, D., Charest, H., Desnoyers, G., Dust, K., Fattouh, R., et al. (2020). Real-time PCR-based SARS-CoV-2 detection in Canadian laboratories. J. Clin. Virol. *128*, 104433. https://doi.org/10.1016/j.jcv.2020.104433.
50. Lu, X., Wang, L., Sakthivel, S.K., Whitaker, B., Murray, J., Kamili, S., Lynch, B., Malapati, L., Burke, S.A., Harcourt, J., et al. (2020). US CDC Real-time reverse transcription PCR panel for detection of severe acute respiratory syndrome coronavirus 2. Emerg. Infect. Dis. *26*, 1654–1665. https://doi.org/10.3201/eid2608.201246.
51. Corman, V.M., Landt, O., Kaiser, M., Molenkamp, R., Meijer, A., Chu, D.K., Bleicker, T., Brünink, S., Schneider, J., Schmidt, M.L., et al. (2020). Detection of 2019 novel coronavirus (2019-nCoV) by real-time RT-PCR. Euro Surveill. *25*, 2000045. https://doi.org/10.2807/1560-7917.ES.2020.25.3.2000045.
52. Gagnier, M., Laurion, I., and DeNicola, A.J. (2020). Control and surveillance operations to prevent chronic wasting disease establishment in free-ranging white-tailed deer in Québec, Canada. Animals *10*, 283. https://doi.org/10.3390/2Fani10020283.
53. World Organization for Animal Health (2020). Considerations for Sampling, Testing, and Reporting of SARS-CoV-2 in Animals. https://www.oie.int/app/uploads/2021/03/a-sampling-testing-and-reporting-of-sars-cov-2-in-animals-3-july-2020.pdf.
54. Di Tommaso, P., Chatzou, M., Floden, E.W., Barja, P.P., Palumbo, E., and Notredame, C. (2017). Nextflow enables reproducible computational workflows. Nat. Biotechnol. *35*, 316–319. https://doi.org/10.1038/nbt.3820.
55. Ewels, P.A., Peltzer, A., Fillinger, S., Patel, H., Alneberg, J., Wilm, A., Garcia, M.U., Di Tommaso, P., and Nahnsen, S. (2020). The nf-core framework for community-curated bioinformatics pipelines. Nat. Biotechnol. *38*, 276–278. https://doi.org/10.1038/s41587-020-0439-x.
56. Patel, H., Varona, S., Monzón, S., Espinosa-Carrasco, J., Heuer, M.L., Nf-Core Bot, Underwood, A., Gabernet, G., Ewels, P., MiguelJulia, et al.. (2022). Nf-Core/Viralrecon: Nf-Core/viralrecon v2.5 - Manganese Monkey. https://doi.org/10.5281/ZENODO.3901628.
57. Chen, S., Zhou, Y., Chen, Y., and Gu, J. (2018). fastp: an ultra-fast all-in-one FASTQ preprocessor. Bioinforma. Oxf. Engl. *34*, i884–i890. https://doi.org/10.1002/imt2.107.
58. Langmead, B., and Salzberg, S.L. (2012). Fast gapped-read alignment with Bowtie 2. Nat. Methods *9*, 357–359. https://doi.org/10.1038/nmeth.1923.
59. Pedersen, B.S., and Quinlan, A.R. (2018). Mosdepth: quick coverage calculation for genomes and exomes. Bioinformatics *34*, 867–868. https://doi.org/10.1093/bioinformatics/btx699.
60. Danecek, P., Bonfield, J.K., Liddle, J., Marshall, J., Ohan, V., Pollard, M.O., Whitwham, A., Keane, T., McCarthy, S.A., Davies, R.M., and Li, H. (2021). Twelve years of SAMtools and BCFtools. GigaScience *10*, giab008. https://doi.org/10.1093/gigascience/giab008.
61. Li, H., Handsaker, B., Wysoker, A., Fennell, T., Ruan, J., Homer, N., Marth, G., Abecasis, G., and Durbin, R.; 1000 Genome Project Data Processing Subgroup (2009). The Sequence Alignment/Map format and SAMtools. Bioinformatics *25*, 2078–2079. https://doi.org/10.1093/bioinformatics/btp352.
62. Grubaugh, N.D., Gangavarapu, K., Quick, J., Matteson, N.L., De Jesus, J.G., Main, B.J., Tan, A.L., Paul, L.M., Brackney, D.E., Grewal, S., et al. (2019). An amplicon-based sequencing framework for accurately measuring intrahost virus diversity using PrimalSeq and iVar. Genome Biol. *20*, 8. https://doi.org/10.1186/s13059-018-1618-7.
63. Cingolani, P., Platts, A., Wang, L.L., Coon, M., Nguyen, T., Wang, L., Land, S.J., Lu, X., and Ruden, D.M. (2012). A program for annotating and predicting the effects of single nucleotide polymorphisms. SnpEff. Fly (Austin) *6*, 80–92. https://doi.org/10.4161/2Ffly.19695.
64. Cingolani, P., Patel, V.M., Coon, M., Nguyen, T., Land, S.J., Ruden, D.M., and Lu, X. (2012). Using Drosophila melanogaster as a model for genotoxic chemical mutational studies with a new program. Front. Genet. *3*, 35. https://doi.org/10.3389/fgene.2012.00035.
65. Elbe, S., and Buckland-Merrett, G. (2017). G. Data, disease and diplomacy: GISAID's innovative contribution to global health. Glob. Chall. *1*, 33–46. https://doi.org/10.1002/gch2.1018.
66. Khare, S., Gurry, C., Freitas, L., Schultz, M.B., Bach, G., Diallo, A., Akite, N., Ho, J., Lee, R.T., Yeo, W., et al. (2021). GISAID's Role in Pandemic Response. China CDC Wkly. *3*, 1049–1051. https://doi.org/10.46234/ccdcw2021.255.
67. Shu, Y., and McCauley, J. (2017). GISAID: Global initiative on sharing all influenza data – from vision to reality. Euro Surveill. *22*, 30494. https://doi.org/10.2807/2F1560-7917.ES.2017.22.13.30494.
68. Turakhia, Y., Thornlow, B., Hinrichs, A.S., De Maio, N., Gozashti, L., Lanfear, R., Haussler, D., and Corbett-Detig, R. (2021). Ultrafast Sample placement on Existing tRees (USHER) enables real-time phylogenetics for the SARS-CoV-2 pandemic. Nat. Genet. *53*, 809–816. https://doi.org/10.1038/s41588-021-00862-7.
69. Kruczkiewicz, P. (2023). CFIA-NCFAD/Delta-SARS-CoV-2-WTD-QC: 1.0.0 - Zenodo Release. https://doi.org/10.5281/zenodo.8364956.
70. Aksamentov, I., Roemer, C., Hodcroft, E., and Neher, R. (2021). Nextclade: clade assignment, mutation calling and quality control for viral genomes. J. Open Source Softw. *6*, 3773. https://doi.org/10.21105/joss.03773.
71. Nguyen, L.-T., Schmidt, H.A., von Haeseler, A., and Minh, B.Q. (2015). IQ-TREE: A fast and effective stochastic algorithm for estimating maximum-likelihood phylogenies. Mol. Biol. Evol. *32*, 268–274. https://doi.org/10.1093/molbev/msu300.
72. Minh, B.Q., Schmidt, H.A., Chernomor, O., Schrempf, D., Woodhams, M.D., von Haeseler, A., and Lanfear, R. (2020). IQ-TREE 2: New models and efficient methods for phylogenetic inference in the genomic era. Mol. Biol. Evol. *37*, 1530–1534. https://doi.org/10.1093/molbev/msaa015.
73. Kalyaanamoorthy, S., Minh, B.Q., Wong, T.K.F., von Haeseler, A., and Jermiin, L.S. (2017). ModelFinder: fast model selection for accurate phylogenetic estimates. Nat. Methods *14*, 587–589. https://doi.org/10.1038/nmeth.4285.
74. Cock, P.J.A., Antao, T., Chang, J.T., Chapman, B.A., Cox, C.J., Dalke, A., Friedberg, I., Hamelryck, T., Kauff, F., Wilczynski, B., and de Hoon, M.J.L. (2009). Biopython: freely available Python tools for computational molecular biology and bioinformatics. Bioinforma. Oxf. Engl. *25*, 1422–1423. https://doi.org/10.1093/bioinformatics/btp163.
75. Minh, B.Q., Nguyen, M.A.T., and von Haeseler, A. (2013). Ultrafast approximation for phylogenetic bootstrap. Mol. Biol. Evol. *30*, 1188–1195. https://doi.org/10.1093/molbev/mst024.
76. Nasir, J.A., Kozak, R.A., Aftanas, P., Raphenya, A.R., Smith, K.M., Maguire, F., Maan, H., Alruwaili, M., Banerjee, A., Mbareche, H., et al. (2020). A comparison of whole genome sequencing of SARS-CoV-2 using amplicon-based sequencing, random hexamers, and bait capture. Viruses *12*, 895. https://doi.org/10.3390/v12080895.
77. Dobin, A., Davis, C.A., Schlesinger, F., Drenkow, J., Zaleski, C., Jha, S., Batut, P., Chaisson, M., and Gingeras, T.R. (2013). STAR: ultrafast universal RNA-seq aligner. Bioinforma. Oxf. Engl. *29*, 15–21. https://doi.org/10.1093/bioinformatics/bts635.
78. O'Hara, E., Herbst, A., Kommadath, A., Aiken, J.M., McKenzie, D., Goodarzi, N., Skinner, P., and Stothard, P. (2022). Neural transcriptomic signature of chronic wasting disease in white-tailed deer. BMC Genom. *23*, *69*. https://doi.org/10.1186/s12864-022-08306-0.
79. Bushnell, B. (2014). BBMap: A Fast, Accurate, Splice-Aware Aligner. https://www.osti.gov/biblio/1241166.
80. Wood, D.E., Lu, J., and Langmead, B. (2019). Improved metagenomic analysis with Kraken 2. Genome Biol. *20*, 257. https://doi.org/10.1186/s13059-019-1891-0.
81. Lu, J., Breitwieser, F.P., Thielen, P., and Salzberg, S.L. (2017). Bracken: estimating species abundance in metagenomics data. PeerJ Comput. Sci. *3*, e104. https://doi.org/10.7717/peerj-cs.104.
82. Patro, R., Duggal, G., Love, M.I., Irizarry, R.A., and Kingsford, C. (2017). Salmon provides fast and bias-aware quantification of transcript expression. Nat. Methods *14*, 417–419. https://doi.org/10.1038/nmeth.4197.
83. Love, M.I., Huber, W., and Anders, S. (2014). Moderated estimation of fold change and dispersion for RNA-seq data with DESeq2. Genome Biol. *15*, 550. https://doi.org/10.1186/s13059-014-0550-8.
84. Sherman, B.T., Hao, M., Qiu, J., Jiao, X., Baseler, M.W., Lane, H.C., Imamichi, T., and

Chang, W. (2022). DAVID: a web server for functional enrichment analysis and functional annotation of gene lists (2021 update). Nucleic Acids Res. *50*, W216–W221. https://doi.org/10.1093/nar/gkac194.

85. Emms, D.M., and Kelly, S. (2019). OrthoFinder: phylogenetic orthology inference for comparative genomics. Genome Biol. *20*, 238. https://doi.org/10.1186/s13059-019-1832-y.
86. Liberzon, A., Birger, C., Thorvaldsdóttir, H., Ghandi, M., Mesirov, J.P., and Tamayo, P. (2015). The Molecular Signatures Database (MSigDB) hallmark gene set collection. Cell Syst. *1*, 417–425. https://doi.org/10.1016/j.cels.2015.12.004.
87. Edgar, R.C. (2004). MUSCLE: multiple sequence alignment with high accuracy and high throughput. Nucleic Acids Res. *32*, 1792–1797. https://doi.org/10.1093/nar/gkh340.
88. Stamatakis, A. (2014). RAxML version 8: a tool for phylogenetic analysis and post-analysis of large phylogenies. Bioinformatics *30*, 1312–1313. https://doi.org/10.1093/bioinformatics/btu033.
89. Kosakovsky Pond, S.L., and Frost, S.D.W. (2005). Not so different after all: a comparison of methods for detecting amino acid sites under selection. Mol. Biol. Evol. *22*, 1208–1222. https://doi.org/10.1093/molbev/msi105.
90. Weaver, S., Shank, S.D., Spielman, S.J., Li, M., Muse, S.V., and Kosakovsky Pond, S.L. (2018). Datamonkey 2.0: A modern web application for characterizing selective and other evolutionary processes. Mol. Biol. Evol. *35*, 773–777. https://doi.org/10.1093/molbev/msx335.
91. Agresti, A., and Coull, B.A. (1998). Approximate is Better than "Exact" for Interval Estimation of Binomial Proportions. Am. Stat. *52*, 119–126. https://doi.org/10.2307/2685469.
92. Statistics Canada (2017). Population and Dwelling Count Highlight Tables, 2016 Census. https://www12.statcan.gc.ca/census-recensement/2016/dp-pd/hlt-fst/pd-pl/Table.cfm?Lang=Eng&T=101&S=50&O=A#2016A000224.

STAR★METHODS

KEY RESOURCES TABLE

REAGENT or RESOURCE	SOURCE	IDENTIFIER
Biological samples		
White tailed deer nasal swabs	This study	N/A
White tailed deer retropharyngeal lymphnodes	This study	N/A
Critical commercial assays		
NUCLISENS® EASYMAG® Reagents	bioMérieux	Cat# 280130-280135
Luna Universal one-step rt-qpcr kit	NEB	Cat# E3005L
MagMax CORE Nucleic Acid Purification Kit	ThermoFisher Scientific	Cat# A32700
TaqMan Fast Virus 1-step Master Mix	ThermoFisher Scientific	Cat# 4444434
LunaScript RT SuperMix	NEB	Cat# E3010
Q5® High-Fidelity DNA Polymerase	NEB	Cat# M0491
Sample Purification Beads	Illumina	Cat# 20060057
Qubit 1X dsDNA HS Assay Kit	ThermoFisher Scientific	Cat# Q33230
Qubit RNA HS	ThermoFisher Scientific	Cat# Q32852
Illumina DNA Prep	Illumina	Cat# 20060059
Illumina DNA/RNA UD Indexes	Illumina	Cat# 20027213, 20027214, 20042666, 20042667
High Sensitivity RNA ScreenTape	Aligent Technologies	Cat# 5067-5579
NEBNext rRNA Depletion Kit v2 (Human/Mouse/Rat)	NEB	Cat# E7405
NEBNext Ultrea II RNA Library Prep Kit for Illumina	NEB	Cat# E7765
dsDNA High Sensitivity chip	Aligent Technologies	Cat# 5067-4626
Quant-iT dsDNA high-sensitivity	ThermoFisher Scientific	Cat# Q33120
NEBNext Library Quant Kit for Illumina	NEB	Cat# E7630L
Deposited data		
White tailed deer SARS-CoV-2 sequences (deposited to GISAID)	This study	EPI_ISL_10169675, EPI_ISL_10170149, EPI_ISL_10168587
White-tailed deer metatranscriptomic sequencing data (deposited to the NCBI Short Read Archive)	This study	BioProject accession no. PRJNA1025888
Experimental models: Cell lines		
Vero E6 cells	ATCC	CRL-1586; RRID: CVCL_0574
Oligonucleotides		
GTTGCAGCCGATCATCAGC	LeBlanc et al.[49]	SARS-CoV-2 5′ UTR Forward Primer
GACAAGGCTCTCCATCTTACC	LeBlanc et al.[49]	SARS-COV-2 5′ UTR Reverse Primer
CGGTCACACCCGGACGAAACCTAG	LeBlanc et al.[49]	SARS-COV-2 5′ UTR Probe
ACAGGTACGTTAATAGTTAATAGCGT	Lu et al.[50]	SARS-COV-2 E gene Forward Primer
ATATTGCAGCAGTACGCACACA	Lu et al.[50]	SARS-COV-2 E gene Reverse Primer
ACACTAGCCATCCTTACTGCGCTTCG	Lu et al.[50]	SARS-COV-2 E gene Probe
TTACAAACATTGGCCGCAAA	Corman et al.[51]	SARS-COV-2 N2 gene Forward Primer
GCGCGACATTCCGAAGAA	Corman et al.[51]	SARS-COV-2 N2 gene Reverse Primer
ACAATTTGCCCCCAGCGCTTCAG	Corman et al.[51]	SARS-COV-2 N2 gene Probe

(*Continued on next page*)

Continued

REAGENT or RESOURCE	SOURCE	IDENTIFIER
AGATTTGGACCTGCGAGCG	Lu et al.[50]	Human RNAseP Forward Primer
AGCGGCTGTCTCCACAAGT	Lu et al.[50]	Human RNAseP Reverse Primer
TTCTGACCTGAAGGCTCTGCGCG	Lu et al.[50]	Human RNAseP Probe
ATGCGGCTAATCCCAACCT	Sequences available from Asuragen	Arm-Ent-31 Forward
CGTTACGACAGGCCAATCACT	Sequences available from Asuragen	Arm-Ent-31 Reverse
CAGGTGGTCACAAAC	Sequences available from Asuragen	Arm-Ent-31 Probe
ARTIC primer pools	https://github.com/artic-network/artic-ncov2019/V3	v3
ARTIC primer pools	https://github.com/artic-network/artic-ncov2019/V4	v4
Recombinant DNA		
Armored RNA Enterovirus	Asuragen	42050
Software and algorithms		
nf-core/viralrecon: nf-core/viralrecon Nextflow workflow	https://github.com/nf-core/viralrecon	V2.2
FastQC	https://www.bioinformatics.babraham.ac.uk/projects/fastqc/	v0.11.9, v0.11.4; RRID: SCR_104583
Fastp	https://github.com/OpenGene/fastp	v0.20.1, v0.21.0; RRID: SCR_016962
Bowtie2	https://github.com/BenLangmead/bowtie2	v2.4.2; RRID: SCR_016368
Mosdepth	https://github.com/brentp/mosdepth/releases	v0.3.1; RRID: SCR_018929
Samtools	https://github.com/samtools/samtools/releases/	v1.12; RRID: SCR_002105
iVar	https://github.com/andersen-lab/ivar	v1.3.1; RRID: SCR_024045
SnpEff	http://pcingola.github.io/SnpEff/	v5.0; RRID: SCR_005191
SnpSift	http://pcingola.github.io/SnpEff/	v4.3t; RRID: SCR_015624
Pangolin	https://github.com/cov-lineages/pangolin/	v3.1.17
UShER	https://github.com/yatisht/usher/tags	v0.6.2
Nextalign	https://github.com/neherlab/nextalign	v2.13.0
IQ-TREE	https://github.com/iqtree/iqtree2	v2.2.0.3; RRID: SCR_017254
BioPython	https://github.com/biopython/biopython	v1.79; RRID: SCR_007173
Nexclade	https://github.com/nextstrain/nextclade	v2.13.0
FigTree	http://tree.bio.ed.ac.uk/software/figtree/	v1.4.4; RRID: SCR_008515
Inkscape	https://inkscape.org/	v.1.0.2; RRID: SCR_014479
STAR	https://github.com/alexdobin/STAR	v2.5.2b; RRID: SCR_004463
BBMap	https://jgi.doe.gov/data-and-tools/software-tools/bbtools/	v38.96; RRID: SCR_016965
Kraken 2	https://github.com/DerrickWood/kraken2	v2.1.2; RRID: SCR_005484
Bracken	https://github.com/jenniferlu717/Bracken/releases	v2.6.0
R	https://www.r-project.org/	v4.1.1; RRID: SCR_001905
Salmon	https://github.com/COMBINE-lab/salmon/releases	v1.4; RRID: SCR_017036
DESeq2	https://bioconductor.org/packages/release/bioc/html/DESeq2.html	v1.34.0; RRID: SCR_015687
OrthoFinder	https://github.com/davidemms/OrthoFinder/releases	v2.5.2; RRID: SCR_017118
MUSCLE	http://www.drive5.com/muscle/	v3.8.425; RRID: SCR_011812
Stata/SE	http://www.stata.com	15.1; RRID: SCR_012763
QGIS	http://www.qgis.org	3.28.2; RRID: SCR_018507
CFIA-NCFAD/Delta-SARS-CoV-2-WTD-QC	https://github.com/CFIA-NCFAD/Delta-SARS-CoV-2-WTD-QC	1.0.0

RESOURCE AVAILABILITY

Lead contact

Further information and requests for resources and reagents should be directed to and will be fulfilled by Samira Mubareka (samira.mubareka@sunnybrook.ca).

Materials availability

This study did not generate new unique reagents.

Data and code availability

- Sequence data from the three SARS-CoV-2 viruses from white-tailed deer sequenced in this study are deposited in GISAID (https://www.gisaid.org/) under Accession numbers EPI_ISL_10169675 (hCoV-19/Canada/QC-WTD-qxic4205/2021), EPI_ISL_10170149 (hCoV-19/Canada/QC-WTD-qxic4249/2021), and EPI_ISL_10168587 (hCoV-19/Canada/QC-WTD-qxic4055/2021). All white-tailed deer metatranscriptomic sequencing data for this project was deposited into the NCBI Short Read Archive (SRA) under BioProject accession no. PRJNA1025888.
- All codes used in this study is available at the sources referenced in the key resources table.
- Any additional information required to reanalyze the data reported in this paper is available from the lead contact upon request.

EXPERIMENTAL MODEL AND SUBJECT DETAILS

Ethical statement

Samples were collected post-mortem from white-tailed deer (WTD) harvested by hunters as a part of the regular annual WTD hunting and not for the purpose of this study. As such, no wildlife collection permit was required by the Ministère de l'Environnement, de la Lutte contre les changements climatiques, de la Faune et des Parcs.

Research ethics approval for the previously analyzed human RNA-seq transcriptomics dataset[25] was approved by the Sunnybrook Research Ethics Board (Transcriptomic analysis in patients with COVID-19; SUN-5024).

Sample collection and study region

White-tailed deer were sampled during the scheduled hunting season after harvesting by licensed hunters. Samples were collected at two big game registration stations in Dunham and Brownsburg, Québec (Figure S1) when harvested and cleaned carcasses were presented for registration; carcasses were returned to the hunters after sampling. Thus, no clinical or post-mortem examination was possible. No animals were killed for the purpose of this study. The Brownsburg station included collection of retropharyngeal lymph node (RPLN) tissues for Chronic Wasting Disease surveillance conducted by the Ministère de l'Environnement, de la Lutte contre les changements climatiques, de la Faune et des Parcs (MELCCFP) in free-ranging WTD in Québec in early November 2021.[52] All samples were collected post-mortem. We collected nasal swabs in 1 mL in-house transport media and retropharyngeal lymph node (RPLN) tissues were collected in dry 2 mL tubes; both sample types were stored at -80°C prior to analysis. Sex, life stage (juvenile or adult) and geographic location of harvest (latitude and longitude) were recorded for each animal. There were 203 males, 53 females, and 2 deer of unknown sex. There were 237 adults, 20 juveniles, and 1 deer of unknown age.

Cells lines

Vero E6 cells, African green monkey cells, from the American Type Culture Collection (ATCC) were maintained in Dulbecco's modified Eagle medium (DMEM) supplemented with 10% fetal bovine serum (Sigma-Aldrich) and 1x l-glutamine and penicillin/streptomycin (Pen/Strep; Corning). All cells were incubated at 37C with 5% CO2.

METHOD DETAILS

Biosafety

All work involving live SARS-CoV-2 was performed in the Combined Containment Level 3 Unit (C-CL3 Unit) of the Temerty Faculty of Medicine at the University of Toronto in accordance with institutional biosafety requirements. Personnel conducting the experiment received containment level 3 training.

RT-PCR screening and detection

RNA extractions were performed using 140 μL of nasal swab sample spiked with Armored RNA enterovirus (Asuragen; https://www.asuragen.com) via the Nuclisens EasyMag using Generic Protocol 2.0.1 (bioMérieux Canada Inc., St-Laurent, QC, Canada) according to manufacturer's instructions. Tissue samples were thawed, weighed, minced with a scalpel, and homogenized in 600 μL of lysis buffer using the Next Advance Bullet Blender (Next Advance, Troy, NY, USA) and a 5 mm stainless steel bead at 5 m/s for 3 minutes. RNA from 30 mg tissue samples was extracted via the Nuclisens EasyMag using Specific Protocol B 2.0.1; RNA was eluted in 50 μL. Reverse-transcription polymerase chain reaction

(RT-PCR) was performed using the Luna Universal Probe One-Step RT-qPCR kit (New England BioLabs; https://www.neb.ca). Two gene targets were used for SARS-CoV-2 RNA detection: the 5′ untranslated region (UTR) and the envelope (E) gene.[49,51] The cycling conditions were: 1 cycle of denaturation at 60°C for 10 minutes then 95°C for 2 minutes followed by 44 amplification cycles of 95°C for 10 seconds and 60°C for 15 seconds. Quantstudio 3 software (Thermo Fisher Scientific; https://www.thermofisher.com) was used to determine cycle threshold (Ct). All samples were run in duplicate and samples with cycle thresholds (Ct) < 40 for both SARS-CoV-2 targets and armored RNA enterovirus in at least one replicate were considered positive. Positive samples were further analyzed for a human RNase P gene target to rule out potential contamination.[50]

Original material from positive samples was sent to the Canadian Food Inspection Agency (CFIA) for confirmatory RT-PCR testing and reporting to the World Organization for Animal Health (WOAH).[53] Total RNA spiked with Armored RNA enterovirus was extracted using the MagMax CORE Nucleic Acid Purification Kit (ThermoFisher Scientific) and the automated KingFisher Duo Prime magnetic extraction system. The enteroviral armored RNA was used as an exogenous extraction control. Confirmatory RT-qPCR was performed using primers and probe specific for both SARS-CoV-2 E and nucleocapsid (N) genes.[50] Master mix for qRT-PCR was prepared using TaqMan Fast Virus 1-step Master Mix (ThermoFisher Scientific) according to manufacturer's instructions. Reaction conditions were 50°C for 5 minutes, 95°C for 20 seconds, and 40 cycles of 95°C for 3 seconds then 60°C for 30 seconds. Runs were performed by using a 7500 Fast Real-Time PCR System (Thermofisher, ABI). Samples with Ct < 36 for both gene targets were reported to WOAH.

SARS-CoV-2 amplification and sequencing

SARS-CoV-2 whole genome sequencing was performed at Sunnybrook Research Institute (SRI) and analyzed at CFIA. Extracted RNA was reverse transcribed into cDNA; 8 μL RNA was mixed with 8 μL nuclease-free water and 4 μL LunaScript RT SuperMix (New England BioLabs) then incubated at 25°C for 2 minutes followed by an incubation at 55°C for 20 minutes and 95°C for 1 minute before holding at 4°C.

cDNA was amplified using ARTIC v3 primer pools (https://github.com/artic-network/artic-ncov2019). Two separate reactions were prepared by combining 2.5 μL cDNA with 6 μL nuclease-free water, 12.5 μL Q5 Hot Start High-Fidelity 2X Master Mix (New England BioLabs) and 4 μL of 10 μM primer pool 1 or primer pool 2 (Integrated DNA Technologies; https://www.idtdna.com). The PCR cycling conditions included an initial denaturation at 98°C for 30 seconds followed by 35 cycles of 98°C for 15 seconds and 63°C for 5 minutes before holding at 4°C. Both reactions were combined and purified with 1X ratio Sample Purification Beads (Illumina; https://www.illumina.com). The resulting amplicons were quantified using Qubit 1X dsDNA HS Assay Kit (Thermo Fisher Scientific).

Libraries were constructed using Illumina DNA Prep (Illumina) and IDT for Illumina DNA/RNA UD Indexes (Illumina) and sequenced on Illumina MiniSeq using 2x149 paired-end reads. Six negative controls (i.e., two extraction, two RT-PCR, and two library prep controls) are included in each sequencing run and all controls must contain <1% of SARS-CoV-2 genome for the run to pass quality control.

Paired-end Illumina reads for samples RT_PCR-positive samples were analyzed using the nf-core/viralrecon Nextflow workflow (v2.2),[54–56] which performed the following analysis steps: FastQC (v0.11.9) read quality assessment (https://www.bioinformatics.babraham.ac.uk/projects/fastqc/); fastp (v0.20.1) read quality filtering and trimming;[57] read mapping to Wuhan-Hu-1 (GenBank: MN908947.3) SARS-CoV-2 reference sequence with Bowtie2 (v2.4.2);[58] read mapping statistics calculation with Mosdepth (v0.3.1)[59] and Samtools (v1.12);[60,61] ARTIC V3 primer trimming, variant calling and consensus sequence generation with iVar (v1.3.1);[62] variant effect analysis and summarization with SnpEff (v5.0)[63] and SnpSift (v4.3t),[64] respectively; SARS-CoV-2 lineage assignment with Pangolin (v3.1.17).

Phylogenetic analysis was performed with the WTD consensus sequences generated by nf-core/viralrecon and 93 closely related NCBI and GISAID[65–67] sequences identified by UShER[68] using a dataset of 14,323,766 genomes from GISAID, GenBank, COG-UK and CNCB (2023-03-28; https://genome.ucsc.edu/cgi-bin/hgPhyloPlace).[69] Multiple sequence alignment (MSA) was performed with Nextalign (v2.13.0)[70] of the 4 WTD, 91 NCBI, 2 GISAID and Wuhan-Hu-1 (GenBank: MN908947.3) sequences. A maximum-likelihood tree was inferred using IQ-TREE (v2.2.0.3)[71,72] from the Nextalign MSA with Wuhan-Hu-1 reference strain (GenBank: MN908947.3) as the outgroup. The best-fit substitution model was determined by IQ-TREE ModelFinder[73] to be GTR+F+I+I+R5. The IQ-TREE phylogenetic tree was pruned with BioPython to highlight distinct clades and amino acid mutation patterns (v1.79)[74] for visualization with the R ggtree library (v3.2.0);[41] taxa with unique amino acid profiles were maintained with a representative for each unique amino acid profile selected at random. Nexclade CLI (v2.13.0)[70] was used to identify amino acid substitutions and deletions in the sequences.

To investigate phylogenetic placement of the SARS-CoV-2 isolated from the Québec WTD relative to other publicly available WTD sequences, we downloaded all complete SARS-CoV-2 genomes isolated from WTD (n = 520) and mule deer (n = 2) available on GISAID (accessed 2023-08-20). Low coverage records including QC-4204 were excluded from the analysis. The Wuhan-Hu-1 (GenBank: MN908947.3) sequence was included as an outgroup. The MSA and maximum likelihood analysis followed the same procedures described for the general phylogenetic analysis (MSA using Nextalign v.2.13.0; maximum likelihood analysis inferred with IQ-TREE v.2.2.0.3). The best-fit substitution model (GTR+F+I+R4) was determined by IQ-TREE ModelFinder using the Bayesian Information Criterion (BIC). Node support was estimated using the ultrafast bootstrap approximation with 1000 replicates.[75] Tree visualization was performed using FigTree (http://tree.bio.ed.ac.uk/software/figtree/) and Inkscape v.1.0.2 (https://inkscape.org/).

Virus isolation

Virus isolation was performed on RT-PCR-positive nasal swabs in containment level 3 at the University of Toronto. Vero E6 cells were seeded at a concentration of $3x10^5$ cells/well in a six well-plate. The next day, 250 μL of sample with 16 μg/mL TPCK-treated trypsin (New England BioLabs), 2X penicillin and streptomycin and 2X antibiotic-antimycotic (Wisent; https://www.wisentbioproducts.com/en/) was inoculated

onto cells. Plates were returned to a 37°C, 5% CO_2 incubator for 1 hour and rocked every 15 minutes. After 1 hour, the inoculum was removed and replaced with DMEM containing 2% FBS, 6 μg/mL TPCK-treated trypsin, 2X penicillin/streptomycin, and 2X antibiotic-antimycotic. Cells were observed daily under a light microscope for cytopathic effect for 5 days post infection. The RT-PCR assay was used to confirm SARS-CoV-2 isolation from supernatant. Comparison of isolate sequences to their original nasal swab sample was conducted for confirmation: cDNA was amplified using ARTIC v4 primer pools (https://github.com/artic-network/artic-ncov2019) and variant calling results were generated using the SIGNAL (SARS-CoV-2 Illumina GeNome Assembly Line) pipeline v1.5.0;[76] these were then compared to variant calling data for the original samples using this analysis workflow. Sequencing of the original nasal swab samples was conducted before ARTIC v4 primer pools were available. We subsequently implemented and used ARTIC v4 to improve genome completeness.

RNA-sequencing of white-tailed deer nasal swabs

Sufficient material was available for only two RT-PCR positive nasal swab samples (4055, 4249) for RNA-sequencing (RNA-seq). Eight total RNA samples, including two SARS-CoV-2 RT-PCR-positive and six randomly selected RT-PCR-negative samples, were submitted for RNA sequencing (RNA-seq) at the Donnelly Sequencing Centre at the University of Toronto (http://ccbr.utoronto.ca/donnelly-sequencing-centre). DNase-treated total RNA was quantified using Qubit RNA HS (cat # Q32852, Thermo Fisher Scientific Inc., Waltham, USA) fluorescent chemistry and 5 ng was used to obtain the RNA integrity number (RIN) using the High Sensitivity RNA ScreenTape (cat # 5067-5579, Agilent Technologies Inc., Santa Clara, USA). Lowest RIN was 1.5; median RIN score was 3. RNA-seq libraries were prepared from RNA samples (150ng) using the NEBNext rRNA Depletion Kit v2 (Human/Mouse/Rat) (NEB Cat# E7405) in conjunction with NEBNext Ultra II RNA Library Prep Kit for Illumina (NEB Cat# E7765). To facilitate the design of WTD-specific ssDNA probes Custom RNA Depletion primers were designed using the tool https://depletiondesign.neb.com/. These were then substituted for the oligos provided in the kit. Ribosomal RNA-depleted libraries had a mean concentration of 15.2ng/uL. 1uL top stock of each purified final library was run on an Agilent Bioanalyzer dsDNA High Sensitivity chip (cat # 5067-4626, Agilent Technologies Inc., Santa Clara, USA). The libraries were quantified using the Quant-iT dsDNA high-sensitivity (cat # Q33120, Thermo Fisher Scientific Inc., Waltham, USA) and were pooled at equimolar ratios after size-adjustment. The final pool was run on an Agilent Bioanalyzer dsDNA High Sensitivity chip and quantified using NEBNext Library Quant Kit for Illumina (cat # E7630L, New England Biolabs, Ipswich, USA).

The quantified pool was hybridized at a final concentration of 320 pM and sequenced paired end 150bp on the Illumina NovaSeq6000 platform using a SP flowcell at a depth of 100M reads per sample.

RNA-seq bioinformatic analysis of white-tailed deer nasal swabs

Raw reads were trimmed with *fastp* v0.21.0,[57] with a front 9 nucleotide trim for R1 and R2 based on a FastQC v0.11.4 quality inspection. To remove the WTD sequences for microbial profiling, we used STAR v2.5.2b[77] to create an index of *Odocoileus virginianus texanus* (GenBank: GCF_002102435.1; also used as a WTD reference in O'Hara et al.,[78]) with a sjdbOverhang of 100 and align the fastp-processed paired-end reads to this index. WTD-aligned reads were removed with BBMap v38.96 filterbyname.sh.[79] The WTD-removed samples were run against the PlusPF pre-built database from May, 17, 2021, consisting of bacteria, archaea, viruses, human, protozoa, and fungi, with Kraken 2 v2.1.2.[80] Species abundance was computed with Bracken v2.6.0.[81] Distance-based clustering on the species and WTD samples was done with the pheatmap v1.0.12 package in R v4.1.1 and applied to a dot plot displaying the relative abundance of species within the community.

For the differential gene expression analysis, the fastp-process paired-end reads were run in the mapping-based mode against a *Odocoileus virginianus texanus* (GenBank: GCF_002102435.1) decoy-aware (genome as the decoy sequence) transcriptome using Salmon v1.4[82] with the validateMappings setting. The quantification files were imported into R (v4.1.1) and a gene mapping file was created with the makeTxDbFromGFF from the DESeq2 v1.34.0 package.[83] Transcript quantifications were merged to the gene-level with tximport using the lengthScaledTPM setting. Low count genes with less than 10 counts were pre-filtered out to improve DESeq2 performance as recommended in the DESeq2 vignette. The differential gene expression analysis was done with the DESeq2 function based on the RT-PCR test results as factor levels. Variance-stabilizing transformation (VST) normalized gene expression for significantly differentially expressed genes based on the adjusted *p*-value and had a $\log_2$ fold change greater than 3 were displayed with gene expression scaling (done with the scale function) in a heatmap with the pheatmap package. The plotPCA function from the DESeq2 package was used to plot a PCA of the VST transformed gene expression profiles. Genes identified as significantly (adjusted p-value) up or down-expressed were run on the Database for Annotation, Visualization and Integrated Discovery (DAVID)[84] on Oct. 7 2022 to identify functional terms (including Gene Ontology terms) enriched in the significantly up and down-expressed gene set over a WTD genome (GenBank: GCF_002102435.1) background. Notably, these genes and associated processes have been defined using human and mouse studies and as such are used as a surrogate to define likely processes in WTD.

To compare the WTD results with a human cohort, OrthoFinder v2.5.2[85] was run on a WTD (GenBank: GCF_002102435.1) and human (GRCh38.p13) proteome (GenBank: GCF_000001405.39), with the proteins mapped back to gene names. The $\log_2$ fold change values from a previous DESeq2 analysis of RNA-seq human COVID-19 infection gene expression,[25] was compared to the WTD DESeq2 results. Briefly, the human RNA-seq transcriptomics dataset is derived from 50 SARS-CoV-2-positive and 13 SARS-CoV-2 negative individuals; nasopharyngeal swab samples were collected from a clinical cohort in the Greater Toronto Area between October 2020 and October 2021.[25] The SARS-CoV-2 positive individuals include 16 outpatients, 16 hospitalized (non-ICU) patients, and 18 hospitalized ICU patients.[25] The GOBP_INNATE_IMMUNE_RESPONSE human gene set from the Human Molecular Signatures Database (MSigDB) C5: ontology[86] was

used to subset the genes investigated and the correlation between the human and WTD immune system log_2 fold change values was calculated with the cor.test function in R v4.1.1.

IFITM1 comparison within O. virginianus and mammalian IFITM1 phylogenetics

Interferon induced transmembrane protein 1 (*IFITM1*) duplication in other *O. virginianus* genomes (GenBank: GCA_023699985.2 and GenBank: GCA_014726795.1) was confirmed via BLASTN searches of those genomes with the two *IFITM1* sequences (GenBank: NW_018336621.1:109564-110759 and GenBank: NW_018336621.1:c138855-136683 for LOC110149600 and LOC110149612, respectively) from *O. virginianus texanus* (GenBank: GCF_002102435.1). Assemblies Genbank: GCA_000191625.1 and GenBank: GCA_000191605.1 were not included as they were extremely small and only fragments of each *IFITM1* gene were able to be detected. As for the IFITM1 sequences across mammals, the IFITM1 HomoloGene group 74501, that includes human, chimpanzee, macaque, wolf, and cow IFITM1 sequences was aligned with MUSCLE v3.8.425[87] to other similar proteins in Boreoeutheria, including the *O. virginianus texanus* IFITM1 proteins. A RAxML-pthreads v8.2.12[88] tree with the PROTGAMMAAUTO setting and the MRE-based Bootstrapping criterion was generated from the alignment, with JTT likelihood with empirical base frequencies being the best-scoring amino acid model for the tree. A nucleotide alignment including coding sequences from all proteins in the tree, as well as the other *O. virginianus* IFITM1 coding sequences, was created with MUSCLE v3.8.425 and subsequently trimmed to the best conserved length with codon alignment corrected. A Fixed Effects Likelihood analysis[89] on this alignment generated with the Datamonkey Adaptive Evolution Server[90] calculated positions with diversifying selection using the default p value threshold of 0.1.

QUANTIFICATION AND STATISTICAL ANALYSIS

Confidence intervals (CI) for SARS-CoV-2 prevalence of infection were estimated using Stata/SE 15.1 (StataCorp, College Station, Texas, USA; http://www.stata.com) with the Agresti-Coull CI method.[91] Diagnostic data were plotted on a map of southern Québec according to the latitude and longitude of each WTD with human population density[92] and WTD harvesting density data (MELCCFP, unpublished data). Maps were produced via QGIS 3.28.2 (Quantum GIS Development Team; http://www.qgis.org).